ISSN 1063-7729, Astronomy Reports, 2016, Vol. 60, No. 1, pp. 1–42. © Pleiades Publishing, Ltd., 2016.
Original Russian Text © A.A. Boyarchuk, B.M. Shustov, I.S. Savanov, M.E. Sachkov, D.V. Bisikalo, L.I. Mashonkina, D.Z. Wiebe, V.I. Shematovich, Yu.A. Shchekinov, T.A. Ryabchikova, N.N. Chugai, P.B. Ivanov, N.V. Voshchinnikov, A.I. Gomez de Castro, S.A. Lamzin, N. Piskunov, T. Ayres, K.G. Strassmeier, S. Jeffrey, S.K. Zwintz, D. Shulyak, J.-C. Gérard, B. Hubert, L. Fossati, H. Lammer, K. Werner, A.G. Zhilkin, P.V. Kaigorodov, S.G. Sichevskii, S. Ustamuich, E.N. Kanev, E.Yu. Kil'pio, 2016, published in Astronomicheskii Zhurnal, 2016, Vol. 93, No. 1, pp. 3–48.

Scientific Problems Addressed by the Spektr-UV Space Project (World Space Observatory—Ultraviolet)

A. A. Boyarchuk[1], B. M. Shustov[1]*, I. S. Savanov[1], M. E. Sachkov[1], D. V. Bisikalo[1], L. I. Mashonkina[1], D. Z. Wiebe[1], V. I. Shematovich[1], Yu. A. Shchekinov[2], T. A. Ryabchikova[1], N. N. Chugai[1], P. B. Ivanov[3], N. V. Voshchinnikov[4], A. I. Gomez de Castro[5], S. A. Lamzin[6], N. Piskunov[7], T. Ayres[8], K. G. Strassmeier[9], S. Jeffrey[10], S. K. Zwintz[11], D. Shulyak[12], J.-C. Gérard[13], B. Hubert[13], L. Fossati[14], H. Lammer[14], K. Werner[15], A. G. Zhilkin[1], P. V. Kaigorodov[1], S. G. Sichevskii[1], S. Ustamuich[5], E. N. Kanev[1], and E. Yu. Kil'pio[1]

[1]*Institute of Astronomy, Russian Academy of Sciences, ul. Pyatnitskaya 48, Moscow, 119017 Russia*
[2]*Southern Federal University, Rostov-on-Don, 344006 Russia*
[3]*Astro Space Center, Lebedev Physical Institute, Russian Academy of Sciences, Moscow, Russia*
[4]*St. Petersburg State University, St. Petersburg, Russia*
[5]*Universidad Complutense de Madrid, Plaza de Ciencias 3, 28040 Madrid, Spain*
[6]*Sternberg Astronomical Institute, Lomonosov Moscow State University, Moscow, Russia*
[7]*Observational Astronomy, Department of Physics and Astronomy, Uppsala University, Box 516, 751 20 Uppsala, Sweden*
[8]*University of Colorado, Boulder, Colorado, USA*
[9]*Leibniz Institut für Astrophysik Potsdam, An der Sternwarte 16, 14482 Potsdam, Germany*
[10]*Armagh Observatory, College Hill, Armagh BT61 9DG, United Kingdom*
[11]*University of Innsbruck, Technikerstrasse 25/8, A-6020 Innsbruck, Austria*
[12]*Institute of Astrophysics, Georg-August University, Friedrich-Hund-Platz 1, D-37077 Göttingen, Germany*
[13]*Laboratory for Planetary and Atmospheric Physics (LPAP), Université de Liège, Liège, Belgium*
[14]*Space Research Institute, Austrian Academy of Sciences, Schmiedlstrasse 6, 8042, Graz, Austria*
[15]*University of Tübingen, Tübingen, Germany*

Received May 14, 2015; in final form, June 26, 2015

Abstract—The article presents a review of scientific problems and methods of ultraviolet astronomy, focusing on perspective scientific problems (directions) whose solution requires UV space observatories. These include reionization and the history of star formation in the Universe, searches for dark baryonic matter, physical and chemical processes in the interstellar medium and protoplanetary disks, the physics of accretion and outflows in astrophysical objects, from Active Galactic Nuclei to close binary stars, stellar activity (for both low-mass and high-mass stars), and processes occurring in the atmospheres of both planets in the solar system and exoplanets. Technological progress in UV astronomy achieved in recent years is also considered. The well advanced, international, Russian-led Spektr-UV (World Space Observatory—Ultraviolet) project is described in more detail. This project is directed at creating a major space observatory operational in the ultraviolet (115–310 nm). This observatory will provide an effective, and possibly the only, powerful means of observing in this spectral range over the next ten years, and will be an powerful tool for resolving many topical scientific problems.

DOI: 10.1134/S1063772916010017

*E-mail: bshustov@inasan.ru

1. INTRODUCTION

In spite of the substantial complexity of operating space-based astronomical instruments, they have become a necessary part of modern studies of the Universe in recent decades. This is so because the properties of the Earth's atmosphere limit possibilities for ground-based observations to fairly narrow windows of transparency. Observations outside these windows—in the gamma-ray, X-ray, UV, and a substantial part of the infrared and submillimeter ranges—is possible only from space.

UV astronomy occupies a special place among the various wavebands, due primarily to the fact that a large fraction of the observable matter in the Universe is located in a state that can be most effectively characterized using UV spectroscopy. UV spectroscopy provides unique possibilities for studies of the intergalactic medium, in particular, for searches of baryonic dark matter, precise determinations of the chemical composition of the interstellar medium, studies of the inner regions of accretion disks, etc. In some research directions (such as studies of the structure of regions of massive star formation in galaxies, hot coronas, and gaseous tori around planets), UV images can provide important information that is difficult or even impossible to obtain using other techniques. We discuss this further in the following sections. The wide possibilities offered by UV techniques explains why dozens of short-lived space experiments have been carried out and more than 20 longer-lived space observatories fully or partially designed for UV observations have been launched over the past 50 years.

These questions have recently been discussed at a number of major international meetings, such as the conference "Challenges in UV-astronomy", held at the European Southern Observatory in Garching, Germany in October 2013, and the symposium "Next Step in Studying the Ultraviolet Universe: WSO-UV," held in the framework of the 40th COSPAR meeting in Moscow in August 2014. The history of early stages in the development of UV astronomy is described in the review [1], the history of UV spectroscopy in [2], the current status of UV techniques for astronomy and perspectives for the future in [3, 4], as well as Chapter 4 of "Fundamental Space Research, Volume 1: Astrophysics" [5], written by B.M. Shustov.

In recent years, new views have arise of both the topical nature of scientific problems in UV astronomy and promising technologies for UV observations carried out in space.

In the current paper, we discuss modern aspects and perspectives for the development of UV astronomy, focusing on various scientific problems that can be addressed. It is natural to analyze the scientific promise of the Spektr-UV space observatory (World Space Observatory—Ultraviolet) in this context. The launch of the observatory is approaching (2021), and interest in its capabilities is growing in the international astronomical community. Section 2 briefly discusses current and future observational methods in the UV, including observations with Spektr-UV. Sections 3–7 consider topical scientific problems of interest to researchers in UV astronomy, and Section 8 presents the conclusions.

2. PERSPECTIVE PROJECTS IN UV ASTRONOMY. WORLD SPACE OBSERVATORY–ULTRAVIOLET (SPEKTR-UV)

2.1. Perspective Projects in UV Astronomy

We will now discuss various proposals for future UV observatories in order to illustrate characteristic tendencies in the development of methods in UV astronomy. It is obvious that far from all these proposed projects will be realized, but nevertheless, they are all of considerable interest. If we consider projects in order of increasing telescope aperture size, we should begin with projects involving small and medium-sized UV telescopes.

The concept of space UV telescopes that are small but capable of providing an appreciable scientific contribution was proposed in [6]. This could be realized using a very small cubesat-class satellite. The small dimensions of the optics and the possibility of limiting the number of intermediate models and using off-the-shelf components makes the cost of such satellites very moderate (less than 10 million Euro). The main scientific goal is carrying out surveys of regions near bright stars that were not covered by the GALEX UV observatories due to the fact that the GALEX detectors were not intended for operation with bright sources. Somewhat larger instruments include the UVIT telescopes on the Indian space observatory Astrosat, whose launch is planned in the near future [7]. These are two 40-cm telescopes intended for observations (imaging) in the near-UV, far-UV, and optical with a field of view of 0.5° and a resolution of $\sim 1''$.

The MESSIER project is intended for survey observations. MESSIER is a space observatory equipped with a UV telescope with a moderate diameter, intended for UV observations (including L_α). The main focus of the project is observations of the ultra-low surface-brightness Universe, which determines a set of structural requirements for the telescope and receiver block. The three-mirror telescope with a 40-cm aperture and a focal number of $f/2$ has a narrow field of view, $2° \times 4°$, and a

spatial resolution of about 1″/pixel. A mosaic of independent CCD arrays is located in the focal plane of the telescope, each optimized for observations in a specific wavelength range; high quantum efficiencies of up to 80–90% are achieved. There are no moving parts, and the receiver block is used in a scanning regime (determined by the telescope's uniform rotation). Thus, the operational scheme is similar to that used in the GAIA mission. The proposed lifetime of the spacecraft is three to five years, during which time observations covering the entire sky will be carried out. The project is being realized jointly by the European Space Agency and the Chinese Academy of Sciences, with a planned launch date of 2020. This information was presented at the conference "Next Step in Studying the Ultraviolet Universe: WSO-UV" (Garching, 2013).

UV sources with low surface brightness are also targeted by the Small-Explorer-class project "Imaging Spectroscopic Telescope for Origins Surveys" (ISTOS). This 50-cm aperture telescope is intended for the detection and mapping of radiation reflected from the intergalactic medium [8].

Plans for a larger telescope for UV and optical imaging are presented in [9]. The 1-m "Cosmological Advanced Survey Telescope for Optical and UV Research" (CASTOR) is designed to construct wide-angle (covering more than 0.7 square degrees) images at 150–550 nm.

The UVMag project (also known as ARAGO) described in [10], with a 1.3-m UV telescope, is designed for spectropolarimetric measurements of stellar magnetic fields, aimed at determining their characteristics and constructing three-dimensional maps of the corresponding stars and their immediate vicinities.

Thus, most projects involving small and moderate-sized space UV telescopes are intended for UV imaging. This is the case because spectroscopy (and especially high-resolution spectroscopy) requires the collection of many more photons, leading to the need for larger telescopes.

One such larger project is the Galaxy Evolution Spectroscopic Explorer (GESE), which has a 1.5-m telescope ($f/5$) equipped with a multi-objective slit selector (a digital microshutter is used) that makes it possible to obtain low-resolution ($R = 400$) spectra simultaneously in four spectroscopic channels in the UV, blue, red, and near-IR [11]. The scientific goal of the project is to carry out spectral studies of more than a million galaxies, in order to identify evolutionary processes leading to the formation of the Hubble sequence.

Following the success of the Hubble Space Telescope (HST), American scientists have proposed a new 2.4-m UV/optical space telescope outfitted with modern instruments, called the High-ORbit Ultraviolet-visible Satellite (HORUS). This NASA project is currently one of the best developed in UV astronomy. It is expected that HORUS will provide an efficiency in UV image construction a factor of 100 higher, and spectroscopic sensitivity in the UV a factor of 10 higher, than the HST. It is proposed to place HORUS in orbit in the vicinity of the Lagrange point L2 of the Sun–Earth system. This orbit has advantages from the point of view of the temperature and spatial stabilization of the telescope. The HORUS optical scheme provides simultaneously a larger field of view for the camera and efficient high-resolution UV spectroscopy for point-like objects. The scientific program of HORUS includes tasks that require a wide-angle camera and spectrograph. HORUS will be able to carry out observations of galaxies with angular resolution more than a factor of 100 higher than is provided by GALEX and Spitzer. The HORUS project includes a 2.4-m, three-mirror, anastygmatic telescope located at the outer housing, which provides the required screening from direct solar radiation, limits light scattering, and provides the first thermal-stabilization circuit of the telescope. Three optical channels are located behind the main mirror. After entering the camera (Dual Focal Plane Imager), a light ray is split into two beams by a dichroic filter, after which the two beams are focused onto two focal planes. The optical scheme of the tri-mirror anastygmat was chosen to provide the required wide, flat field. The main parameters of the HORUS space project can be found in [12].

A group of Russian astronomers has recently proposed the Astron–2 project, which is a space observatory designed for all-sky spectral and photometric surveys in the UV. The main element of this observatory is a wide-angle UV telescope with a 2-m aperture. The design parameters of the Astron-2 space observatory are appreciably better than those of GALEX, which had a Ritchey–Chrétien telescope with a 50-cm main mirror. The advantages of Astron-2 are possible due to the high photometric sensitivity and accuracy in the UV provided by the use of CCD detectors, which have widely recommended themselves in many space experiments. The expected accuracy of the stabilization of the spacecraft is no worse than 0.03″. Astron-2 will be able to carry out deep photometric and spectral surveys, including of the Galactic plane and regions of the sky containing large numbers of bright objects, which were not accessible by GALEX. Astron-2 observations will enable study of a whole series of important astrophysical problems:

- deep surveys of the stellar populations of tens of thousands of galaxies and mapping of regions of star formation in these galaxies;
- UV observations of millions of distant galaxies aimed at studying their evolution and the star-forming history of the Universe to redshifts $z \sim 2$;
- detailed mapping of interstellar absorption in our Galaxy;
- detailed studies of star-forming regions in our Galaxy;
- astroseismological studies of white dwarfs and O and B subdwarfs; an important research strand is the detection of new planets around such subdwarfs, which will provide information about interactions in star–planet systems at late stages of the evolution of the star;
- studies of various types of brightness variability in young stars in the stage preceding their arrival to the main sequence.

Two ambitious and expensive projects based on the use of large and very large telescopes are being considered for the far future. One scaled-up version of the HST is the Telescope for Habitable Exoplanets and Interstellar/Intergalactic Astronomy (THEIA). NASA is considering this as a worthy successor to the HST, which would also nicely supplement the capabilities of the James Webb Space Telescope (JWST). THEIA is a multi-purpose space observatory operating in the optical and UV [13]. It could be used in a wide range of scientific studies, including imaging of exoplanets and determining their characteristics, and studies of star formation, galaxy formation, and the properties of the interstellar medium. With its wide-angle camera, UV spectrograph, and planetary camera and spectrograph, THEIA will be suitable for studies of a wide range of astronomical questions.

The multi-wavelength Advanced Technologies Large-Aperture Space Telescope (ATLAST, USA) is currently a set of concepts for missions involving new-generation space observatories whose main telescopes have diameters of 8–16 m. Such a mission would make it possible to carry out complex observations, and answer a range of important questions challenging ambitious UV projects, including "Is there other life in the Galaxy?" [14]. Two different types of telescopes are considered for this project, having similar optical schemes: one with a single main mirror and two options with a more segmented main mirror. This approach presents several paths for realizing the project.

European scientists have recently proposed the 4–8-m class European Ultraviolet Observatory (EUVO) [15].

Finally, French scientists have proposed a very interesting telescope project based on the exploitation of Fresnel zones. The proposed instrument is an ultra-light telescope demonstrating new optical concepts based on diffraction focusing [16]. This design makes it possible to obtain high-dynamic-range images, while simultaneously reducing restrictions on the arrangement and manufacture of the main optical elements. This concept could open a path to large apertures (up to 50 m) operating in space. In such a system consisting of two spacecraft, one spacecraft carries the focusing block—a zone Fresnel plate—while the second spacecraft carries the field optics, focal instruments, and detectors. The field of view of the telescope is modest, and it is most efficient for studies of compact objects (e.g., protoplanetary disks) with very high angular resolution.

2.2. Spektr-UV (World Space Observatory—Ultraviolet)

The need for a large-scale UV space observatory is currently critical. The projects described in the previous section are very interesting, but the current reality is that large-scale UV space observatories will be realized no earlier than the end of the 2020s. The time required for planning and constructing an observatory such as the HST or a larger-scale observatory is longer, no less than 15–20 years, and all the proposed large-scale projects above are still in early stages of their development. The in-orbit lifetime of HST itself is currently expected to last until 2018. For the first time in nearly a half century, astronomers will face the problem of access to UV observations. In the period up to the end of the 2020s, the most promising access to the "ultraviolet window" is provided by the Spektr-UV project, leading to considerable interest in this project from the international astronomical community. This began as a project in the "Spektr" series of space observations, designed for observations in the radio (Spektr-R), UV (Spektr-UV), and X-ray (Spektr-RG). At the suggestion of the broad international collaboration, the project also obtained another name: World Space Observatory—Ultraviolet (WSO—UV). This collaboration was ended for financial reasons, and the project is now being realized in Russia with the participation of Spain. The project is included in the Federal Space Program (FSP) of Russia for the period 2016–2025, under both names: Spektr-UV and World Space Observatory—UV, and we accordingly use both names in this paper.

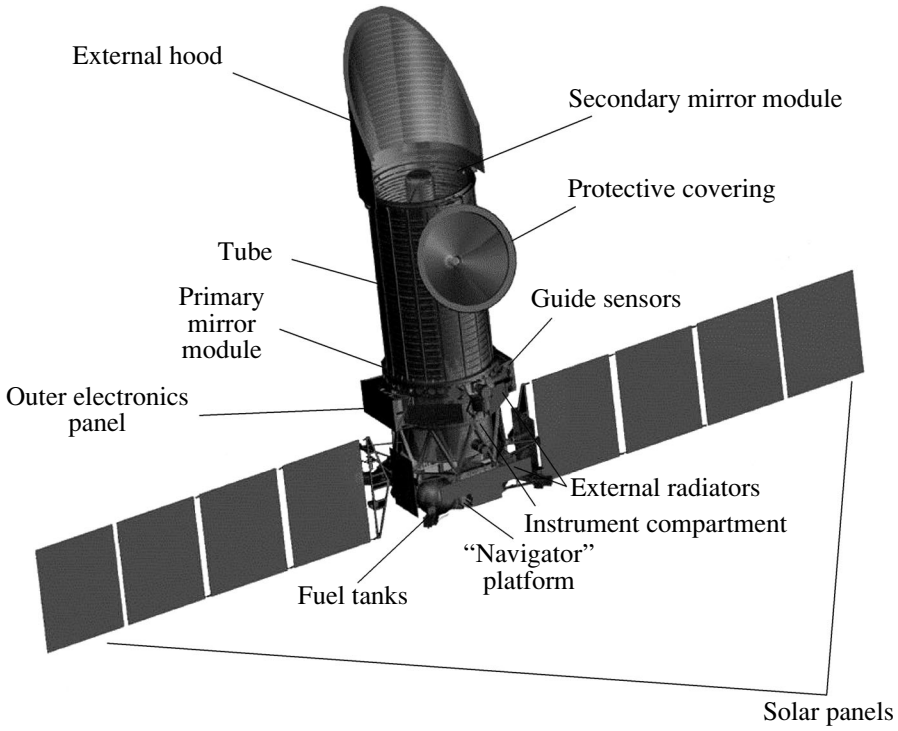

Fig. 1. General appearance of the Spektr-UV spacecraft.

The goal of the Spektr-UV project is to construct a space observatory intended for observations in the near and far UV (115–310 nm). The development of the project is described in [17]. It's main characteristics and a discussion of the scientific program of the Spektr-UV program can be found in [17–20].

In this section, we will briefly summarize the main information about the project, since the main purpose of the current paper is to consider current and future scientific problems in UV astronomy whose solution will be addressed by Spektr-UV.

The main scientific topics addressed by the project (included in the basic program) can be briefly summarized as follows:

- the baryon component of the Universe, the thermal and chemical evolution of the Universe;
- the formation and evolution of our Galaxy, the interaction of gas and stars, and the influence of magnetic fields on star formation;
- the physics of accretion and matter outflows;
- atmospheres of planets (exoplanets).

The Spektr-UV space complex includes the Spektr-UV spacecraft, the associated ground segment, and the rocket space complex. We will not dwell on a description of the rocket space complex and its components, which include the booster, the cosmodrome technical complex, cosmodrome launch complex, a complex for measurement, data-collection, and processing of information during ascent, since these components are standard for all projects. It is planned to launch the Spektr-UV spacecraft using a Proton rocket. We will likewise not dwell on a description of the ground complex.

Figure 1 shows the general appearance of the Spektr-UV spacecraft. The main components include the service module (platform) and the payload, i.e., the scientific complex. A "Navigator" base module is used as the service module. The Navigator module was developed as a universal service module for a number of space projects. The assembly of the Navigator module at the Lavochkin Research and Production Association is shown in Fig. 2. Note that the Lavochkin Association is the leading organization for the space complex, while the leading organization for the scientific complex is the Institute of Astronomy of the Russian Academy of Sciences.

The "RadioAstron" space radio-astronomy observatory (launched into orbit in 2011) and the "Elektro" spacecraft designed to carry out measurements of the Earth from a distance have already been realized on the basis of this service module.

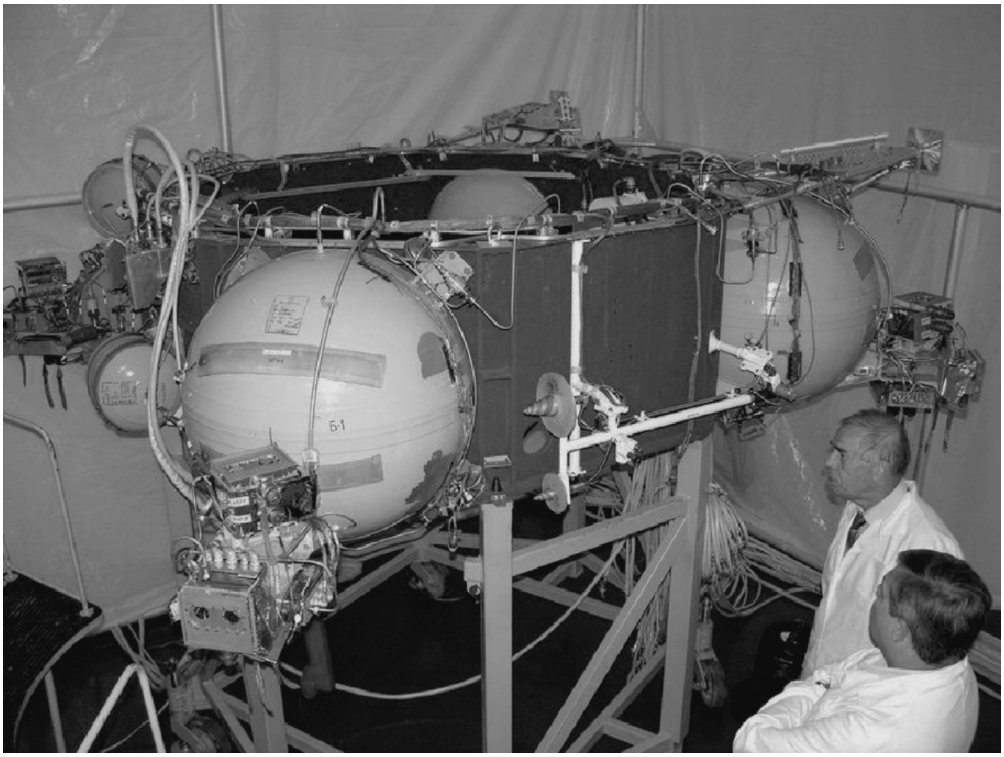

Fig. 2. Assembly of the "Navigator" service module at the Lavochkin Association.

The Spektr-UV scientific complex is optimized for observations at 115–310 nm. In principle, the UV range is much broader, but experience from previous missions (EUVE, ROSAT) indicates that UV observations of astrophysical objects at the short-wavelength end of this range (10–91 nm) are hindered at wavelengths longer than 30 nm by strong absorption by interstellar hydrogen and helium. Unfortunately, the $Al + MgF_2$ coatings used for the optical elements are not efficient at the (extremely interesting astrophysically) wavelengths of 91–110 nm (see the discussion in [21]). The LiF coatings that are efficient in this wavelength range are very complicated to use, leading to the selection of the wavelength range 115–310 nm as a compromise.

The Spektr-UV scientific complex includes:

- the T-170M telescope;
- the main scientific-instrument complex, which contains:
  - the spectrograph block, which includes a vacuum UV photoelectric spectrograph (VUVPS), UV photoelectric spectrograph (UVPS), and long-slit spectrograph (LSS) channels;
  - the field-camera block (FCB);
  - the scientific-data control block (SDCB);
- the "Konus-UV" apparatus—a new version of a small gamma-ray detector developed at the Ioffe Institute, which has already successfully been used in various space experiments.

The scientific complex as a whole is described in [18], and we will present here only some brief information about its characteristics.

Table 1 presents the general characteristics of the T-170M telescope.

Table 1. Main optical parameters of the T-170M telescope

Parameter	Specification
Type of optical system	Ritchy–Chretien
Aperture diameter	1700 mm
Focal ratio	10.0
Diameter of field of view	0.50° (200 mm)
Accessible wavelength range	110–700 nm

Table 2. Main characteristics of the UVPS, VUVPS, and LSS channels of the spectrograph block

UVPS and VUVPS	
Wavelength range	
UVPS	174–305 nm
VUVPS	115–176 nm
Resolving power	∼55 000
LSS	
Wavelength range	115–310 nm
Resolving power	∼1000
Spatial resolution	0.5″–1″

The most important scientific instrument is the spectrograph block. Optical computations were carried out at the Special Astrophysical Observatory of the Russian Academy of Sciences, where the optical scheme of the spectrograph block was composed [22]. The main operational regime of the spectrograph block includes the accumulation and preliminary reduction of spectra of observed objects and, if needed, compression of the resulting observational scientific information. In the main operational regime and during calibration, only one channel of the spectrograph block can function at any given time. The maximum duration of an observing session is 12 hours. Table 2 presents the characteristics of the spectrograph-block channels.

Selected CCD arrays serve as the detectors in all three spectrograph channels. To enhance the quality of the observational material obtained with the CCD detectors and avoid their degradation, a system of glare and heat (annealing) detectors is included.

A key question is estimation of the efficiency of the spectrograph-block channels, determined as the product of the efficiency of each element of the optical scheme for the corresponding channel. First and foremost, this refers to data characterizing the reflective properties of the $Al + MgF_2$ coating on the main and secondary telescope mirrors, the coatings on the dispersive elements/chambers of the spectrograph block, and the flat mirror of the LSS channel; the efficiency of diffraction gratings; and, finally, the efficiency of the CCD detectors.

Figure 3 presents estimates of calculated effective areas for the UVPS, VUVPS, and LSS channels of the spectrograph block, compared to data for the HST Cosmic Origins Spectrograph (COS) and Space Telescope Imaging Spectrograph (STIS). The spectral resolution of the UVPS and VUVPS channels is comparable to the resolution of the STIS with E140 and E230 echelle gratings, but higher than the maximum resolution of the COS ($R = 20\,000$). It is expected that the effective area of the VUVPS in the far ultraviolet will be comparable to the HST instruments, and exceed their effective area in the near UV. We believe this can be achieved thanks to substantial progress in the efficiencies of CCD detectors [23] and the high quality of the UV coatings of the reflecting elements [21]. Note that this high efficiency of the spectographs (channels) can be reached in spite of the fact that the surface area of the T-170M telescope is roughly half the corresponding surface area of the HST.

The field-camera block (FCB) is the other main scientific instrument of the Spektr-UV project. The FCB is intended for the acquisition of high-quality direct UV images of cosmic objects using light filters, as well as images in a low-resolution field-spectroscopy mode (the final decision about whether this mode will be included in the project has not been made). First and foremost, the FCB is intended for studies of weak, point-like or extended UV sources using light filters. The FCB has two essentially identical channels operating in different wavelength ranges: one in the far UV at 115–175 nm, and the other in the near UV at 185–320 nm. Preliminary estimates indicate that the efficiency of the FCB will be close to that of the HST/ACS camera.

3. COSMOLOGICAL PROBLEMS WHOSE STUDY REQUIRES UV OBSERVATIONS

3.1. Ionizing Radiation in the Universe

One of the fundamental problems in modern cosmology is determining the onset of the epoch of reionization—i.e., the onset of the transition from pre-stellar evolution of the Universe (the so-called "dark epoch") to the modern Universe—and investigating the dynamics of this transition, together with its duration and the dependence of the subsequent evolution of the Universe on the characteristics of the reionization. The dynamics of the reionization are determined by two factors: (1) the rate of energy release in the form of hard electromagnetic (mainly UV) radiation by stars during nucleosynthesis, and also by black holes with high accretion rates, and (2) the escape of this energy from galaxies into intergalactic space. Determining the escape fraction of UV photons is a fundamentally important task in observational cosmology. Recently, joint studies based on measurements of the degree of ionization in regions of formation of the so-called L_α forest and modern cosmological modeling have revealed an appreciable—factor of five—deficit of ionizing

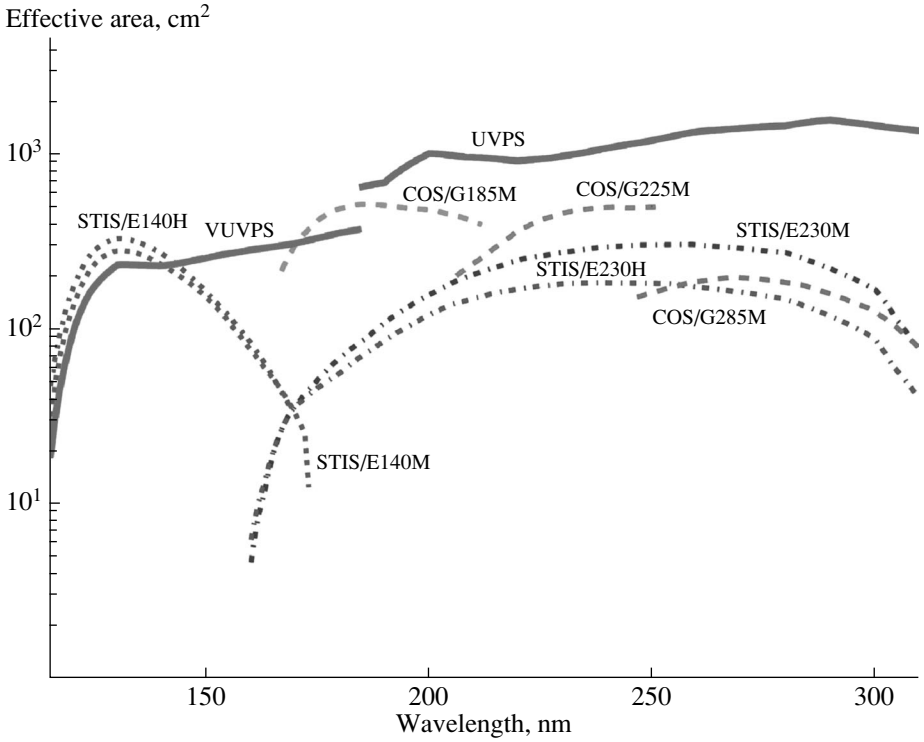

Fig. 3. Effective area of the VUVPS and UVPS channels as a function of wavelength.

photons in the local Universe (at redshifts of about $z = 0.1$), which may indicate fundamental problems of the entire dynamics of reionization [25]. In this sense, searches for ways of observationally determining the fraction of ionizing photons escaping from galaxies even in the local Universe are of fundamental importance. In principle, this issue can be addressed using observations of lines of the Lyman series from diffuse HII regions adjacent to galaxies, produced by Lyman-continuum photons that have left galactic disks.

3.2. The Cosmic History of Star Formation

The cosmic history of star formation $\Psi(z)$ refers to the dependence of the star-formation rate per unit volume of the Universe on the redshift z. This is a fundamental evolutionary characteristic of the post-recombination Universe, since it determines the dynamics of reionization, the chemical evolution of the Universe, the mass spectrum of galaxies at the lower mass limit, etc. However, in spite of efforts spent in recent years and the appearance of new observational data, there are no reliable estimates of $\Psi(z)$ [26], and our overall understanding of the star-formation history of the Universe remains inadequate, due to uncertainties in required corrections for optical extinction in galactic disks. Infrared observations are adversely affected by uncertainties in estimates of the contribution from local sources. As a result, differences in estimates of $\Psi(z)$ in the relatively nearby Universe ($z < 2$) based on optical and infrared observations reach an order of magnitude [27]. One task related to this problem to which Spektr-UV can make a decisive contribution is determining correct estimates of the optical and UV extinction occurring in galactic disks. Such observations could include a careful analysis of differences in the spectral energy distributions in galaxies oriented at various angles to the line of sight.

It is well known that the galaxy luminosity function $\Phi(L)$ shows a strong dependence on the angle of the plane of the galaxy to the line of sight θ for all values of θ, from face-on to edge-on galaxies [28]. This means that the observed optical background carries information about the amount of extinction in galactic disks. Therefore, a careful investigation of the spectrum of the optical background and spectra of galaxies as a function of their orientation to the line of sight can provide information necessary for our understanding of the star-formation history $\Phi(L)$.

3.3. The Intergalactic Medium: Hidden Baryons and the Mixing Problem

Determining the total mass of baryons and heavy elements in the Universe is a key problem. Estimates

obtained in the last few years have brought to light two fundamental problems: "hidden" baryons [29–32] and "hidden" metals [33–37], which have not yet found a satisfactory resolution. The essence of the first problem is that estimates of the observed baryonic mass at redshifts $z \geq 2$ are in agreement with the distribution of light elements formed via cosmological nucleosynthesis and with WMAP data ($\Omega_b \simeq 0.04$), but estimates at the current epoch ($z \sim 0$) indicate values about a factor of two lower. A similar problem arises for estimates of the mass of heavy elements: computations of the expected mass of heavy elements that should be produced by stars in the Universe, beginning from the first episodes of stellar nucleosynthesis up to the current epoch, are appreciably higher than indicated by observations of the amount of heavy elements in galaxies and galaxy clusters. Many modern space projects are directed toward carrying out a "full inventory" of baryonic matter in the Universe, such as the Athena [38] and DIOS [39] X-ray projects.

Possible reservoirs of the "hidden" matter that have been discussed include a warm–hot phase of intergalactic gas with temperatures $T = 10^5$–10^7 K [40–42] and extended circumgalactic gaseous halos [43, 44]. Studies carried out over the past few years have demonstrated the presence of gaseous halos around galaxies, extending to distances of up to 200 kpc and having masses that can be comparable to the stellar mass in the galactic disk. Hopes for detecting warm–hot intergalactic gas rely on observations of absorption lines of highly charged ions such as OVI and OVII [45]. However, due to the weakness of these lines, which are close to the instrumental limits, firm detections are fairly rare. Moreover, in cases when absorption in OVI/OVII lines is detected, this is not confirmed by X-ray observations [46, 47]. However, a fundamentally weak aspect of such observations is that they are always based on certain assumptions about the distribution of heavy elements and their ionization state.

There is currently no doubt that mixing of metals in the diffuse intergalactic medium and the interstellar medium is inefficient. Moreover, the character of the spatial distribution of metals appears to display a certain correlation between metallicity and the characteristic size of the region containing the metals, namely: small condensations contain more metallic gas, as is testified by both numerous numerical simulations [48] and observations of metallicity in the intergalactic medium at $z \simeq 3$ [49]. Thus, determining the metallicity of intergalactic gas from absorption lines can be subject to observational selection effects due to the fact that small condensations that are more saturated in metals can be relatively difficult to detect, due to their small geometrical cross sections. One consequence of this observational selection effect is that the mass of metals will be systematically underestimated.

In this regard, the Spektr-UV project can make a determining contribution to resolving this problem. Specifically, it can enable the following:

- observations of new and known regions of warm–hot intergalactic gas and extended halos around galaxies with high spectral resolution;
- detailed studies of the dependence of metallicity on the size and other physical characteristics of regions containing metals, making it possible to correctly take into account observational selection effects due to possible correlations between metallicity and size.

4. THE INTERSTELLAR MEDIUM AND STAR FORMATION

4.1. Chemical Composition of the Interstellar Gas: The Mixing Problem

The chemical composition of the interstellar gas, i.e., its metallicity and the relative abundances of various elements, is of fundamental importance for the molecular composition and thermodynamics of the interstellar medium and characteristics of star formation. As was already noted in Section 3, it has recently become clear that mixing of chemically inhomogeneous material ejected by massive stars and supernovae require times that are long, even by galactic scales. The first model numerical computations showed that mixing of matter on scales of the order of about 1 kpc could require more than 100 million years [50]. Analysis of the chemical composition of the stars HDE 226868 (the optical component in Cyg X-1) and α Cam shows that mixing in the interstellar medium within 2 kpc of the Sun could require more than one billion years [51] (see also [52]). Modern hydrodynamical numerical computations of mixing of metals in a diffuse cosmic medium on various scales have shown that, in most cases, the efficiency of mixing is limited by saturation, when the degree of mixing "freezes" at some level that depends on specific dynamical conditions [53, 54].

Studies of inhomogeneity of the chemical composition of the interstellar gas taking into account these factors is a fundamental task for improving our understanding of the physics of the interstellar medium. A program of such studies organized as part of the Spektr-UV project could include surveys, or at least scanning of selected regions, in absorption lines of ions such as OI, OII, CII, CIII, CIV, SiIV, FeII, and MgII. The strongest (resonance) lines of these

elements fall in the UV; this is true, for example of CII ($\lambda = 1036-2325$ Å), OI ($\lambda = 919-1355$ Å), MgII ($\lambda = 1026-1240$ Å), SiII ($\lambda = 1190-2335$ Å), and FeII ($\lambda = 1055-1901$ Å). Such studies could be carried out in directions where the effects of incomplete mixing would be most appreciable and would admit a relatively simple interpretation. A prime example of such a region is the local interstellar medium (the "Local Bubble"). Studies of metals and their relative abundances in old (such as Vela and Simeiz) and young (the Crab, SN 1006, and others) supernova remnants, and investigation of the spatial distributions of metals as a function of age, are also relevant here. Studies of the distributions of the speeds of ions and atoms of various elements (O, C, Si, Fe, Mg) with high spectral resolution along selected lines of sight near the Sun (for example, in the region studied in [51]) could also provide interesting results on the dynamics of mixing of metals.

4.2. Dark Molecular Gas

Another fundamental problem concerning the physics of the interstellar medium for which observations with Spektr-UV could prove decisive is estimating the total mass of atomic and molecular gas in the Galaxy. Numerous data on the existence of so-called CO dark gas have appeared recently (see, e.g., [55]). The possibility that a substantial fraction (up to 70% by mass) of CO could be dark, i.e., unobservable in rotational lines of CO, was first expressed in [56]. This possibility is related to the fact that the transformation of atomic to molecular hydrogen as gas is compressed begins appreciably earlier than the binding of C and O into CO molecules, due to self-screening. Therefore, surveys in H_2 Lyman absorption lines will be of fundamental importance not only for estimates of the masses of molecular hydrogen that is invisible in CO lines, but also for studies of the vicinities of the nearest molecular clouds, and constructing spatial profiles of the H_2 distribution, investigating the relationship between the number densities of H_2 and CO in transitional regions, etc. This will lead to a better understanding of the kinetics of molecularization of the interstellar gas, and enable the identification of factors determining the dependence of the coefficient $X(\mathrm{CO})$ for converting emission in CO lines into an H_2 number density on the physical conditions and phase state of the gas.

4.3. Tiny Scale Atomic Structures

Another class of interstellar object, Tiny Scale Atomic Structures (TSAS) [57–59], could also contain a substantial amount of "uncounted" gas in the interstellar medium. Tiny-scale clouds with sizes from several to several thousands of AU appear to be short-lived objects (with lifetimes of several hundreds of years). Their typical temperatures are those of molecular clouds, $T \sim 10-20$ K, and the number density of the gas they contain is $n \sim 10^2-10^5$ cm^{-3}. Such clouds must thus be appreciably pre-Jeans; since their internal pressures are either comparable to the external pressure in the interstellar medium or appreciably exceed this external pressure at the upper end of their number densities, they are unstable, and have lifetimes of hundreds of years. The "frequency" of these structures, i.e., the rate at which they appear in absorption spectra, is fairly high: their relative total geometrical cross section (surface factor) is, on average, about 40% of the celestial sphere, and their volume filling factor could reach 0.2% [58]. This could imply that these condensations contain a mass comparable to the mass of diffuse HI gas. However, interpretations of the phenomenon of TSAS clouds are fairly vague, due in good part to insufficient statistics about their properties. For example, they could represent fragments interacting with the local interstellar medium (the Local Bubble), or fragments surrounding clouds of molecular hydrogen (see the discussion in [57–59]). In either case, their properties reflect fundamental dynamical phenomena accompanying interactions of shocks from numerous supernovae, as occurs in the Local Bubble, or the dynamics of the formation of molecular clouds; i.e., they characterize the state of the interstellar medium as a whole in the Galaxy.

TSAS could be associated with small-scale motions, i.e., motions on scales of several AU, manifest in interstellar scintillations and extremely scattering events in the radio [60]. Recent data indicate that the structures responsible for interstellar scintillation and extreme scattering events could reflect the existence of a continuous background of electron-density fluctuations [61]. The characteristic scales corresponding to these phenomena are of order an AU or less, which, in turn, correspond to the scales for the dissipation of interstellar turbulence [62]. Studies of these structures are also therefore of undoubted interest for our understanding of interstellar turbulence and the phenomena determining its dissipation.

Dissipation of turbulent structures has been proposed as a possible explanation for the relatively high molecular content in the diffuse interstellar medium [63]. Spectral observations in the UV provide a unique opportunity to study the absorption lines of molecules such as CO, N_2, OH, C_2, and some others (apart from molecular hydrogen). UV spectra are also a possible source of information about the abundance of deuterized molecular hydrogen, HD [64]. Observations with Spektr-UV will make

it possible to appreciably increase the number of directions in which the abundance of this molecule has been measured, helping to elucidate its role in the chemistry of both diffuse media and denser molecular clouds. As a whole, observations of molecular UV absorption lines will make it possible to determine whether these molecules are initial reagents of more complex chemical processes in the formation of molecular clouds or, on the contrary, represent products of the dissipation of compact molecular clumps. Accompanying UV observations of absorption lines of neutral and ionized carbon will enable detailed studies of the properties not only of the transition $H \rightarrow H_2$, but also the transition $C^+ \rightarrow C \rightarrow CO$ [65]. C_2 observations could prove important for studies of diffuse interstellar bands (DIBs).

UV emission lines of H_2 and the ion CIV can also be used as sources of information about the structure and mass of interstellar matter in star-forming regions and near massive stars [66, 67].

4.4. Properties of Interstellar Dust

Observations of interstellar absorption lines can be used not only to determine the abundances of various elements in the gaseous phase, but also to estimate their abundance in dust, by comparing the abundances of atoms and ions in the gas phase with their overall cosmic abundances. This will make it possible to appreciably reduce uncertainties associated with the choice of a model for interstellar dust, since all interstellar dust grains are currently believed to consist of the same five "important" elements: C, O, Mg, Si, and Fe. Unfortunately, elemental abundances have been measured for a very small number of directions in our Galaxy: O, Mg, and Fe for 120–150 stars, Si for ~40 stars, and C for ~20 stars [68, 69]. In general, observations have been carried out only for bright stars with modest absorption ($A_V \lesssim 1.5^{\rm m}$), for many of which the UV interstellar absorption curves are unknown.

Determining UV absorption curves could also become an important research direction, since this information is required for determining the chemical compositions and sizes of dust grains. Studies of variations of the so-called UV hump in the absorption curve at wavelength 2175 Å [70], which is considered to be a key indicator of the nature of cosmic dust grains, are of special interest. Thus far, interstellar absorption in the UV has been measured for only a few hundred stars, mainly with $A_V \lesssim 3.0^{\rm m}$ [71, 72].

The overall problem of investigating metal abundances in the interstellar medium can be summarized as follows. The abundances of the five elements listed above (C, O, Mg, Si, Fe) must be determined in various directions, paying particular attention to the closest stars ($D \lesssim 400$ pc) with substantial absorption ($A_V \gtrsim 3.0^{\rm m}$). Observations with high spectral resolution are required for this purpose. Simultaneous low-resolution spectroscopy in those same directions can be used to determine interstellar absorption curves. Note that precise determinations of the silicon abundances in the directions of stars with measured interstellar polarization could help test the hypothesis that only silicate particles give rise to polarization [73]. A comparison of the distribution of UV absorption and elemental abundances in various parts of the Galaxy will help place additional constraints on mechanisms for the growth of interstellar grains [74].

5. PHYSICS OF ACCRETION AND OUTFLOWS IN ASTROPHYSICAL OBJECTS, FROM GALACTIC NUCLEI TO CLOSE BINARY SYSTEMS

Studies of the accretion of gas onto compact objects and stars and related outflows represent an important part of modern theoretical and observational astrophysics. These processes are crucial for our understanding of star formation, the nature of active galactic nuclei, including quasars, and the observational properties of compact objects such as black holes, neutron stars, white dwarfs, etc. Moreover, studies of accretion processes and associated outflows provide unique opportunities to investigate the behavior of matter under conditions of very high temperatures, as well as extremely strong magnetic and gravitational fields, which is fundamentally impossible under terrestrial conditions.

Since many accreting systems radiate an appreciable fraction, or even the bulk, of their energy in the UV, this spectral range is especially important for our understanding of processes occurring in accreting gas, and also for determining the parameters of the accreting objects. Here, we will discuss only a few topics related to the physics of accretion and outflows in astrophysical objects. When selecting topics to include, our criteria were the interest for the overall scientific community, and the existence of appreciable discrepancies between theoretical concepts and observational results (in particular, in the UV). Such problems can be resolved only by obtaining further observational data, for example, with the Spektr-UV space observatory, and a full consideration also requires further development of the relevant theory. For convenience of the reader, we will divide each section into two parts, corresponding to a consideration of a particular problem as it relates to extragalactic sources and to objects in our Galaxy.

5.1. Extragalactic Accretors as Sources of Powerful UV Radiation

5.1.1. UV excess in the continuum spectra of quasars and Active Galactic Nuclei (the Big Blue Bump). An important feature in the spectra of quasars and Active Galactic Nuclei (AGNs) is a powerful rise in the spectrum at wavelengths near 1000 Å, which is identified with radiation of an optically thick, geometrically thin accretion disk (see, e.g., [75]). Although theoretical computations of the spectra of accretion disks (see, e.g., [76]) based on the standard model of Shakura and Syunyaev [77] and the relativistic generalization by Novikov and Thorne [78] have met with some success, including a qualitative explanation for the behavior of the spectra in the optical and infrared, the theory and observations are not in agreement in the UV.

Let us briefly discuss the main problems arising when modeling the UV spectra of quasars and AGNs (see, e.g., [79, 80]). First, the position of the maximum UV radiation in theoretical models depends on both the ratio of the accretion flux to the Eddington limit and the mass of the black hole, while observations show that the maximum UV radiation in most AGNs is located near 1000 Å in the source rest frame. Moreover, the theoretical typical temperatures for the inner regions of the disk are appreciably higher than is observed. Second, even if we suppose that the observations yield correct temperatures, the resulting relatively soft spectrum is not sufficient to ionize gas clouds in the broad-line region, whose presence is implied by the broad lines in the spectra of quasars and AGNs. An illustration of the discrepancies between theory and observations is given in Fig. 4.

Apart from these main problems, there also remain a whole series of other unresolved questions, such as the time scale for variability of the radiation, the wavelength dependence of the variability, etc. Some of these problems can be eased in less standard theoretical approaches, which propose, for example, the presence of an optically thick gas cloud at a distance of several tens of gravitational radii from the black hole [79], gas outflows due to radiation pressure in lines [81] or accretion and outflows due to radiation pressure in the continuum for near-Eddington or super-Eddington disks (see, e.g., [80, 82]. However, there is no generally accepted explanation for the observed discrepancies, presumably due to an insufficient volume of observations of quasars and AGNs in the UV. In order to accumulate the required statistics, the observations should encompass a large number of systems realizing various accretion modes and containing black holes with various masses, rotational parameters, and inclinations of the accretion disks to the line of sight. Analysis of the observations must take into account not only the continuum spectrum associated with the disk, but also emission lines arising in the broad-line region. It stands to reason that the theory of accretion disks around supermassive black holes must be developed accordingly.

5.1.2. Phenomena arising due to tidal disruption of stars by supermassive black holes. Tidal-disruption events due to supermassive black holes (Fig. 5) are associated with flares emitted from the center of an inactive galaxy and the subsequent decrease in its luminosity, as a rule on time scales of order several years. It is generally believed that the drop in intensity should follow a power law ($t^{-5/3}$), although modern computations show that the fall-off in intensity should have a more complex character (see, e.g., [84]). About 30 such events have currently been measured [85], and this number should increase substantially over the coming few years. Note that solar-type stars can be disrupted by supermassive black holes of moderate mass ($\leq 10^8 - 10^9\ M_\odot$), where the exact mass depends on the rotation of the black hole and the orientation of the stellar orbit (see [86] and references therein), while more massive black holes can disrupt less dense stars, such as red giants. The detection and study of tidal-disruption events is not only important for our understanding of the physics of non-stationary accretion processes and determining the parameter of the associated black holes, but is also very important for establishing the character of the distribution of stars in phase space near black holes, which determines the rate of tidal disruptions.

Currently, most such events are detected in the soft X-ray, although three were discovered in the UV [85]. Note that the number of events in the UV could be larger than those in the X-ray if a suitable observing strategy is chosen and it is possible to detect fairly weak intensities. In fact, it follows from the standard theory of disk accretion that the characteristic temperature of the radiation should fall off as the matter flux decreases, as $\dot{M}^{2/5}$ for a Thomson-thick disk in which the gas pressure dominates the radiation pressure. Since the characteristic temperature of the disk on time scales of several years (for definiteness, one year) is about 1 keV $\approx 10^7$ K and $\dot{M} \propto t^{-5/3}$, we find a temperature of 30 000 K, corresponding to a wavelength of 100 nm, will be achieved in 6000 yrs. It is obvious that there will be 1000 time more objects with their maximum luminosity in the UV than those with their maxima in the X-ray. However, the luminosity of these objects will be lower by approximately a factor of 10^6. Given that the luminosity will be close to the Eddington luminosity for a black hole with a mass of $10^7 M_\odot$ (i.e., $\simeq 10^{45}$ erg/s) on a time scale of about a year, we find that the luminosity should be $\simeq 10^{39}$ erg/s after

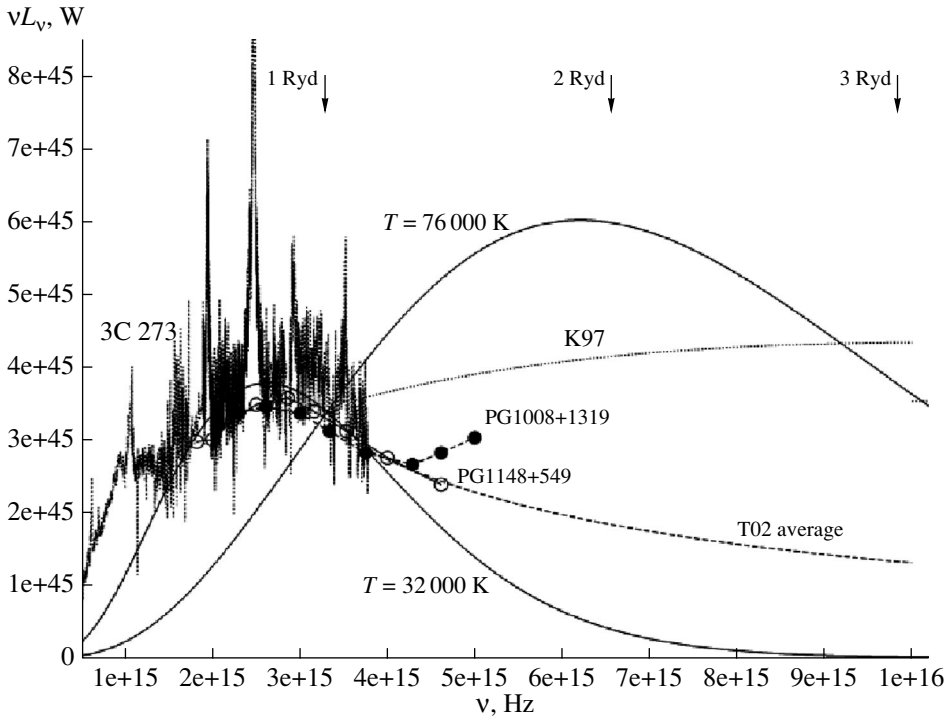

Fig. 4. Comparison of the observed flux density of the quasar 3C 273 with various theoretical model predictions. The circles show the observed continuum flux density. The solid curve labeled $T = 32\,000$ K shows a fit to the continuum spectral flux density with blackbody radiation corresponding to a temperature of 32 000 K, and the solid curve labeled $T = 76\,000$ K the theoretically expected flux density for such an object. The dotted curve K97 shows the flux density required for sufficient ionization of the broad-line region. The dashed curve T02 corresponds to an averaged power-law spectrum with index −1.8. The continuous spectrum is indented by lines formed in this zone. Taken from [79].

6000 yrs. Therefore, searches for such "late" stages in the evolution of accretion disks formed after a tidal-disruption event should be carried out for fairly nearby galaxies and with fairly long exposure times.

5.1.3. Binary supermassive black holes. An interesting object whose presence is reliably predicted theoretically is binary supermassive black holes (see, e.g., [87, 88]). Mergers of binary supermassive black holes leads to the appearance of powerful sources of gravitational radiation (see, e.g., [89]), and their interactions with gas to the appearance of non-standard, non-stationary radiation from the centers of the galaxies at various wavelengths, including the UV.

The simple theory of the interaction of a binary supermassive black hole with an accretion disk around the more massive black hole predicts two qualitatively different stages [90]. In the first, the orbit of the less massive black hole is inclined to the plane of the accretion disk and the black hole passes through the disk twice in each orbital period. An outflow of optically thick, radiatively dominated gas forms as a result of these passes through the disk [91]. The luminosity of this gas is of order the Eddington luminosity of the lower-mass black hole, and the peak emission occurs in the soft X-ray or UV. In the second stage, the orbital period and the plane of the disk coincide. If the less massive black hole moves in the direction of rotation of the gas in the disk, a rarified cavity forms inside the binary orbit. Otherwise, when the mass ratio is low, a gap forms along the orbit of the less massive black hole (see [92] and references therein).

In both cases, a certain amount of gas accretes onto both black holes, with this process being non-stationary, with a characteristic variability time scale of the order of the orbital period. When there is a cavity inside the orbit, the spectrum has a characteristic "notch" [93]. The position of this notch in frequency depends on the accretion rate in the disk and the size of the orbit, but, when the mass flux is not very low compared to the Eddington value and the orbital radius is of order hundreds of gravitational radii, this notch is located in the UV, at wavelengths near 1000–2000 Å. The character of the accretion onto the less massive black hole for the case when it moves opposite to the rotation of the gas in the disk has not been established, but it seems reasonable to suppose that the peak emission will again occur in

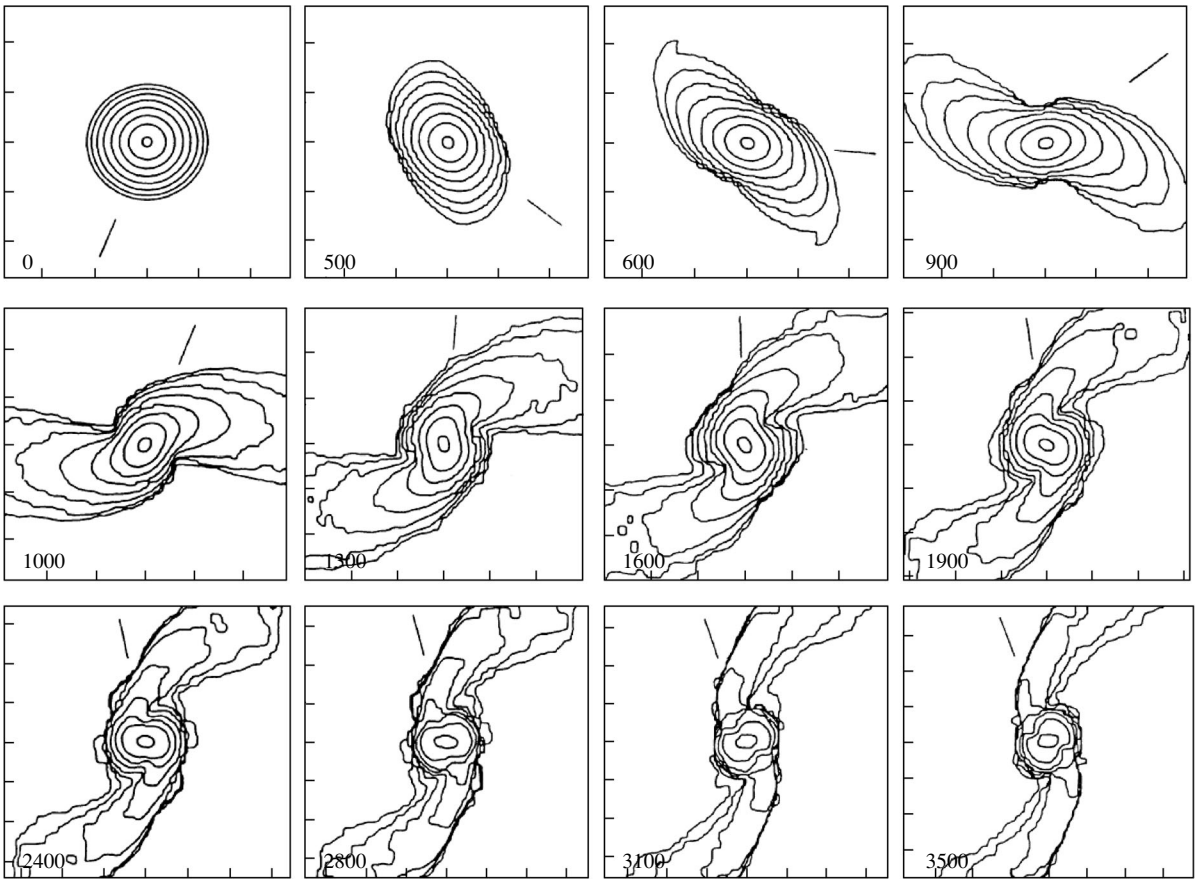

Fig. 5. Contours of constant density for a star disrupted by a black hole projected onto the orbital plane. A time in computational units is indicated in each panel; the line segment indicates the direction toward the black hole. For stars with solar parameters, one computation time unit is approximately 1.6 s. The star passes through periastron approximately at time $t = 400$ in computational units. Further, the density distribution acquires a characteristic S-like form. The star was modeled as a polytrope with index $n = 3$ and adiabatic index $\gamma = 5/3$. Taken from [83].

the soft X-ray and UV. The accretion onto the more massive black hole is similar to that discussed above, except that periodic modulation of the emission will be observed.

Perhaps the best known candidate for a binary supermassive black hole is the BL Lac object OJ 287, which demonstrates variability in its luminosity with a period of about 12 years. The nature of this variability is sometimes explained using phenomena arising when the less massive black hole passes through the accretion disk [94], and the UV excess that is observed at the flare maximum is believed to be related to the outflow of hot plasma from the disk. There are also several other binary supermassive black hole candidates, based on possible periodicity of their observed fluxes, such as the quasars PG 1302-102 [95] and PSO J334.2028+01.4075 [96], but there is no reliable identification with binary supermassive black holes. Note also that binary supermassive black holes could be detected in the optical and UV using other methods; for example, two spectrally distinct systems of broad emission lines should arise in objects in which there is an accretion disk around each of the black holes, due to the orbital motion of the black holes. The spectrum of the quasar SDSS J153636.22+044127.0 has been interpreted in this way [97].

Therefore, searches for such objects in the UV are very important. Their detection would make it possible to estimate the number of binary supermassive black holes yielding flares of gravitational radiation—required for planning future space-based gravitational-wave antennas—and also elucidate many aspects of the physics of accretion, the formation of large-scale structure and galaxies in the Universe, and the formation of supermassive black holes themselves.

5.1.4. Ultrabright X-ray sources and microquasars. Ultrabright X-ray sources are a group of extragalactic objects located outside centers of galaxies and radiating in the X-ray range with typical

luminosities of $10^{39}-10^{40}$ erg/s, which exceeds the Eddington limit for a solar-mass body. Their nature is not yet clear. They are most likely a varied group of objects. Some are probably black holes or neutron stars in binary systems that are accreting super-Eddington mass fluxes, and others may be intermediate-mass black holes ($10^2-10^4\ M_\odot$). In the former case, the super-Eddington luminosity is explained by collimation of the radiation arising in the gas outflow that arises naturally at such high accretion rates (see, e.g., [98]). In the latter case, the objects obviously have sub-Eddington luminosities. Note that the reliable detection of intermediate-mass black holes is extremely important, since it would shed light on the processes involved in the formation of black holes. In particular, this would answer the long-standing question of whether a black hole can form in a globular cluster.

The first type of ultrabright X-ray source is essentially a so-called "microquasar," of which a typical representative is the well known object SS 433 (see, e.g., [99]). The peak radiation in such objects occurs in the UV and corresponds to a characteristic temperature of 50 000–70 000 K; differences in their properties are explained as the effect of different orientations of the accretion disk and outflow relative to the line of sight. Analogous models have been proposed for other ultrabright X-ray sources as well [100]. Observations in the UV could be used to search for microquasars in other galaxies. On the other hand, models for ultrabright X-ray sources in which the accretor is taken to be an intermediate-mass black hole generally predict other spectral properties, with the spectral peak in the X-ray and typical UV fluxes several orders of magnitude below the peak flux (see, e.g., [101]). Therefore, a deficiency of UV emission for a particular object could provide evidence that it is an intermediate-mass black hole.

Many ultrabright X-ray sources are surrounded by regions of order hundreds of parsecs in size that gives rise to optical line emission (see, e.g., [102]. It is believed that the mechanism exciting these lines is either photoionization by an X-ray or UV continuum or ionization by shocks. It is of interest to search for such lines in the UV, since their presence and properties could help elucidate which of these competing models is more suitable for a given source.

5.2. Accreting Sources of Powerful UV Radiation in Our Galaxy

5.2.1. Binary systems containing black holes or neutron stars. The accretion disks around black holes and neutron stars in binary systems radiate mainly in the X-ray, although observations in the UV are also very important. Moreover, in many systems, the donor is a massive, hot star radiating in the UV. Observations of the continuum and lines of this star can be used to determine important characteristics of the system, such as its orbital parameters, distance, the mass of the optical star, the type of accretion, the star's rotational period, etc. For example, the donor in the classical binary with a black hole Cygnus X-1 is an O supergiant whose properties have been determined from spectroscopic observations in the UV [103]. Many of the ultrabright X-ray sources discussed above are fed by gas ejected by massive, bright stars located in fairly close orbits. Searches for such systems in the UV, determination of their type, etc. can obviously shed light on the nature of ultrabright X-ray sources.

The technique for determining the component separation based on joint observations in the X-ray and in induced fluorescent optical and UV radiation is of interest. In principle, the time delays between variations in the outer regions of the disk in the different spectral ranges can be used to deduce the component separation [104]. On the other hand, UV observations in the continuum and in lines arising due to the irradiation of the disk by X-rays provide important information about the properties of the accretion disk—the accretion rate, outer radius, dependence of the disk thickness on radius, etc. (see, e.g., the discussion of these questions in [105], with applications to the source Sco X-1).

5.2.2. Non-magnetic cataclysmic variable stars. Cataclysmic variable stars are binary systems where one component (as a rule, a red dwarf) fills its Roche lobe, leading to an outflow of its matter through the vicinity of the inner Lagrange point L_1, with its subsequent accretion onto the secondary component, which is a white dwarf (see, e.g., [106]). The angular momentum of the matter that leaves L_1 is too high for the matter to fall directly onto the compact star, leading to the formation of an accretion ring at some (comparatively small) distance from the accretor [107]. Under the action of dissipative processes, this ring gradually spreads and forms an accretion disk, whose inner boundary is directly adjacent to the accretor. Some of the matter at the outer boundary of the disk can leave the system through the vicinity of the Lagrange point L_3, carrying away excess angular momentum and forming an intercomponent envelope (see, e.g., [108, 109]). Gas-dynamical processes occurring in the accretion disk and envelope lead to the formation of a complex flow pattern, including a whole series of stationary shocks, as well as a set of non-stationary and quasi-stationary elements contributing to the emission and absorption of the stellar radiation [110–113].

The temperatures of the white dwarfs in cataclysmic variables can reach 10^5 K, with a large fraction of the energy radiated in the UV. The temperatures of the accretion disks can also lie in the range 10^4-10^5 K. The peak radiation for such temperatures lies in the range ~300–3000 Å, which corresponds well to the spectral range of Spektr-UV [114]. The processes in cataclysmic variables proceed on various time scales, from so-called flickering on time scales of the order of several seconds to superflares lasting tens of days. The most important time scale for observations is the orbital period of the system, which usually ranges from several hours to days. Spektr-UV will enable observations of processes occurring on this time scale with good time resolution.

Observational studies of non-magnetized cataclysmic variables can be divided into several groups, which we will now consider in turn.

a. Flows of matter in the vicinity of the accretor. The region directly adjacent to the surface of the white dwarf is of considerable interest, since it is there that the most intense energy release associated with the accretion occurs. The accreted gas is subject to a large compression in this region, leading to heating and possible flares [115]. UV observations will enable estimation of the density, temperature, and flow structure in the immediate vicinity of the white-dwarf surface, making it possible to test theories for Type Ia flares.

Several different kinds of white dwarfs displaying the presence of pulsations are currently known [116]. The pulsating activity of white dwarfs is directly related to the presence of a remnant hydrogen envelope that influences the cooling of the star (see, e.g., [117]). UV observations can be used to estimate the parameters of this envelope.

The rotation of the white dwarfs could appreciably influence the flow structure in the system [118]. The rotation of the white dwarf can be spun up during interaction with the accretion disk, making the rotational velocity an indicator of the accretion intensity in the past. UV observations can be used to estimate this rotation rate.

In the case of high accretion rates, the luminosity of the white dwarf can approach the Eddington limit [119], which should give rise to a wind from the white dwarf in the presence of an optically thick envelope. The presence of such a wind could have a considerable influence on the mass-transfer rate, and accordingly on the evolution of the system [120]. Analyses of UV spectra and light curves can provide information about the parameters and structure of the wind from the white dwarf.

Information on the structure of the white-dwarf photosphere can be obtained through eclipse mapping when the star is in its quiescent state (see, e.g., [121]). UV light curves and line-profile variations during eclipse can provide information about the distribution of regions of accretion on the white-dwarf surface, making it possible to estimate the strength and configuration of the white-dwarf's magnetic field.

b. Structure of the accretion disk. The flow structure in the Roche lobe of the accretor is very complex (Fig. 6), and can include the accretion disk; a flow of matter from the inner Lagrange point L_1; a circumdisk halo; an extended, stationary shock called a "hot line" that forms when the stream collides with the circumdisk halo; tidal shocks; the outgoing shock ahead of the disk; and a precessional wave in the disk [110–113]. The accretion disks make a substantial contribution to both the emission of the cataclysmic variable and to absorption during eclipse, with the peak of their blackbody radiation lying in the UV.

The planned orbit for Spektr-UV will enable long series of observations, making it possible to obtain series of spectograms covering half the orbital periods of most cataclysmic variables. Such spectrograms can be used to construct Doppler tomograms [122], which can then be used to produce images of the flow pattern in velocity coordinates. Although analyses of Doppler tomograms requires numerical models [123. 124], this method is currently the only one that can yield detailed images of the flow patterns in cataclysmic variables. Three-dimensional Doppler tomographic methods have recently been developed [125, 126], which impose high requirements on the quality of the spectra used, but can be used to reveal the vertical flow patterns in the systems observed. Another method that can be used to obtain the radial distribution of parameters in the disk is eclipse mapping. Variations of the brightness and line profiles can be fitted to derive, for example, information about the temperature distribution in the disk (see, e.g., [127]).

The results of numerical computations show that the accretion disks formed in semi-detached binary systems can be appreciably elliptical [113]. This ellipticity could be a consequence of the presence of a precessional wave in the disk [128], and could appreciably influence the flows in the system [108, 109]. Pronounced eccentricity of the disk could be manifest in Doppler tomograms [124]. UV spectral observations could be used to determine the eccentricities of the accretion disks in cataclysmic variables.

An increasing number of studies have recently been dedicated to SW Sex stars. These are nova-like stars with extremely high mass-transfer rates, giving rise to numerous observational manifestations that do not fit in the standard theoretical framework. For example, the radial-velocity curves of these stars display a cycle shift relative to the light curve (see,

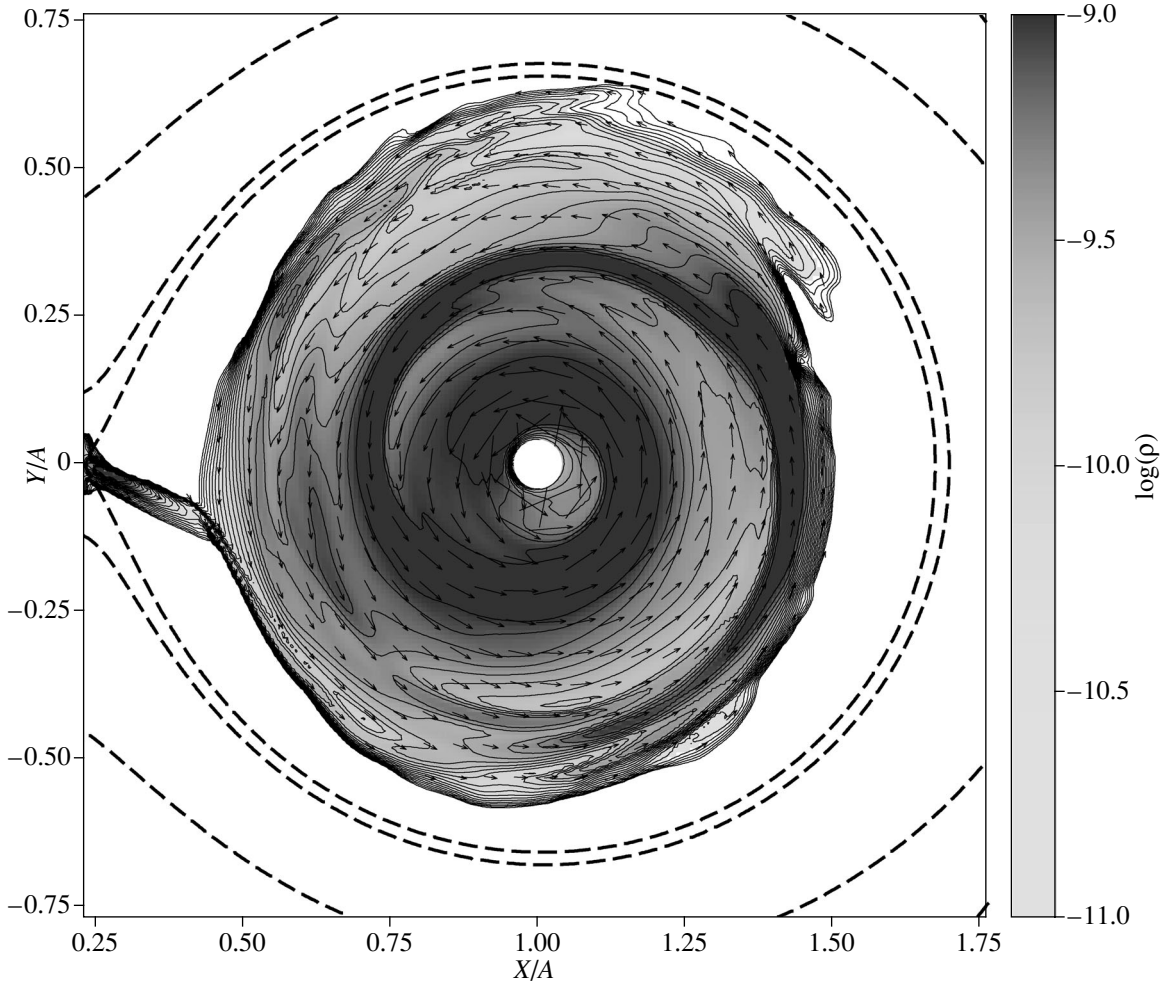

Fig. 6. Distribution of the density and velocity vectors in the accretion disk of a cataclysmic variable star (results of gas-dynamical modeling). The dashed curves show the Roche equipotential.

e.g., [129]). Detailed spectral and photometric observations of such stars with Spektr-UV could help refine the existing theory and provide explanations for the SW Sex phenomenon.

c. Turbulence in accretion disks. The matter leaving L_1 possesses too much angular momentum to fall directly onto the white dwarf. The only mechanism currently known that is able to carry away this excess angular momentum is turbulent viscosity, described using the parameter α of Shakura and Syunyaev [77]. However, no fairly reliable mechanisms leading to turbularization of accretion disks in binary systems are currently known. There are a number of competing hypotheses aiming to explain the development of instability in accretion disks (see, e.g., [130] and references therein), but testing these hypotheses requires additional studies, including new observational data.

The parameters of turbulent flows in accretion disks in binary systems are currently unknown, as is the spectrum of the turbulence. The variability of cataclysmic variables on time scales comparable to the time scale for the revolution of material around the white dwarf (flickering) is usually associated with inhomogeneity of the accreting flow due to turbulence. Studies of this type of variability using Spektr-UV can provide necessary information.

d. Envelopes of cataclysmic variables. As a rule, cataclysmic variables pass through a common-envelope stage at some point in their evolution (see, e.g., [131] and references therein). This mysterious period is too short in duration (of order several years) to be observed directly, although it is very important, since there is a sharp loss of angular momentum from the system due to braking during this stage.

The results of gas-dynamical numerical modeling show that a cataclysmic variable can have an intercomponent envelope formed of matter ejected from the accretion disk [108, 109]. Spektr-UV observa-

tions could be used both to detect remnants of such envelopes ejected in earlier stages of the evolution of the system and to determine the parameters of envelopes forming in the cataclysmic-variable stage.

e. Flares and superflares. One of the most important properties of cataclysmic variables is their flare activity. These systems exhibit several different types of flare, which have been described using various physical mechanisms and various models (see, e.g., [128, 132, 133]). The flares can give rise to substantial variations in the flow structure in the system; in particular, they can lead to disruption of the accretion disk and the possibility of directly observing the white dwarf (see, e.g., [134]). The temperature is enhanced during flares, increasing the short-wavelength radiation, in particular, in the UV. Studies of this flare activity represent an interesting problem whose solution requires both new observational material and the development of theoretical models.

5.2.3. Magnetic cataclysmic variables. The magnetic fields at the surfaces of the white dwarfs in magnetic cataclysmic variables reach values of 10^4-10^8 G. Simple estimates show that the corresponding magnetic moment of the white dwarf in a magnetic cataclysmic variable and a neutron star in an X-ray binary are roughly the same, of order 10^{30} G cm^3. This indicates that the magnetosphere radii for these white dwarfs and neutron stars are roughly equal. However, the component separations in cataclysmic variables are tens, or even hundreds, of times smaller than those in X-ray binaries. Therefore, the influence of the magnetic field on flows of matter and the structure of the accretion disk is overall much stronger in magnetic cataclysmic variables than in X-ray binaries. Two main types of magnetic cataclysmic variables are distinguished: polars and intermediate polars.

a. Polars. The white dwarfs in a polar have strong surface magnetic fields ($>10^6$ G) [135]. The highest magnetic-field strength measured thus far is that in the AN UMa system (230 MG). Polars are characterized by relatively short orbital periods, from one to five hours. Their strong magnetic fields hinder the formation of an accretion disk, leading to synchronization of the rotations of the components [136]. It is believed that the matter overflowing from the donor forms a collimated accretion flow, which falls onto the region of one of the magnetic poles of the accretor along its strong magnetic field lines. An additional source of energy forms in the accretion zone at the base of this accretion channel, with most of the energy released in the X-ray and UV. Since this energy release occurs in the region of a strong magnetic field, this radiation is highly circularly polarized. The spectral distribution of the flux from an accretion column has three main components: (a) hard X-ray radiation from the hot region behind the shock, (2) cyclotron radiation from electrons moving in the strong magnetic field, and (3) reprocessing of absorbed radiation in the UV and soft X-ray.

Due to the interaction of the donor atmosphere with the white-dwarf magnetosphere, the rotational periods of the white dwarfs are equal to the binary orbital periods in most polars [135]. However, a small subset of polars are known as asynchronous polars, or BY Cam stars [137]. These binaries provide additional opportunities for more complete studies of magnetic accretion onto white dwarfs, since the rotational periods of the white dwarfs in asynchronous polars differ only slightly from their orbital periods. The structure of the field is probed by the accretion flow of plasma coming from all sides of the white dwarf, due to the fact that the inner Lagrange point L_1 is located at various azimuthal angles relative to the magnetic field during the spin-orbital beat period.

There is also numerous observational evidence that the geometry of the white-dwarf magnetic field can be more complex than dipolar [138–140]. For example, it was established in [139] that the white dwarf in the EE Eri system has a quadrupolar magnetic field with four accretion spots. The existence of high-order magnetic fields (quadrupolar, octupolar, etc.) in white dwarfs is also confirmed by Zeeman tomography of polars [141, 142]. The magnetic field of the asynchronous polar BY Cam apparently also has a complex geometry. This was first shown in [143, 144], and was convincingly confirmed by subsequent observations. The light curve of this system displays switching, drift of the poles, and even the simultaneous presence of several (three or four) regions of active accretion.

Figure 7 presents the flow structure believed to be present in the BY Cam system, based on the results of three-dimensional computations [112, 145]. This type of solution is fairly typical, and provides an impression of the main features of the flow structures present in the computations that have been carried out. The figure shows surfaces of constant logarithmic density. The main flow corresponds to darker shades. Magnetic field lines with arrows are also shown, together with the rotational axis of the accretor (thin vertical line) and the symmetry axis of the dipolar magnetic field (bold inclined line). The inner Lagrange point L_1 from which matter flows into the accretor's Roche lobe is located on the negative X axis.

b. Intermediate polars. Intermediate polars are magnetic cataclysmic variables with relatively weak magnetic fields (10^4-10^6 G at the surface of the

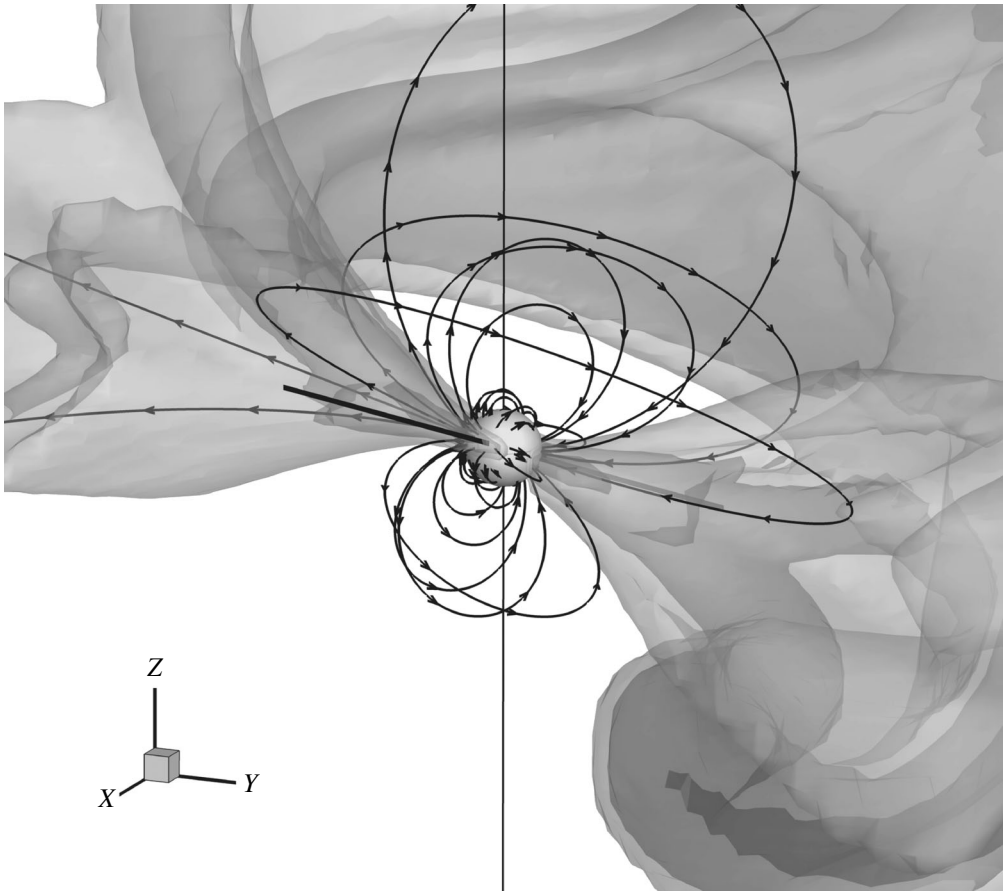

Fig. 7. Results of three-dimensional MHD computations of the flow structure in a polar with a complex magnetic-field geometry. Surfaces of constant logarithmic density and magnetic-field lines are shown. The vertical thin line shows the rotational axis of the accretor, and the inclined bold line the symmetry axis of the dipolar magnetic field.

accretor). They occupy an intermediate position between polars and non-magnetic cataclysmic variables. The orbital periods of intermediate polars display a fairly large amount of scatter, from several hours to several tens of hours. The rotational periods of the accretors in these systems are shorter than their orbital periods by one, two or even three orders of magnitude [136]. In the DQ Her (rapidly rotating) subclass that is sometimes distinguished, this difference between the rotational and orbital periods is even greater. The remaining systems are divided into regular intermediate polars, EX Hya systems, and systems with nearly synchronous rotation, based on the ratio of their periods [136]. The asynchronous nature of the rotation of the accretors in intermediate polars is determined by the interaction of the white-dwarf magnetic field with plasma of the disk at the boundary of the magnetosphere. The accreting matter at the inner edge of the disk penetrates into the white-dwarf magnetic field and, moving along the magnetic-field lines, reaches the white-dwarf surface near the magnetic poles. The energy released as this matter falls onto the surface of the white dwarf is released mainly as X-rays. However, the radiation of the accretion disk itself lies in the optical and UV.

Intermediate polars give rise to specific types of study associated with the structure of the accretion disk. The influence of the white-dwarf magnetic field leads to the formation of an inclined accretion disk [146]. Such disks have been observed, for example, in the TV Col [147], RR Cha [148], XX Tau [149], and XY Ari systems (and others). To explain the shift in phase of the X-ray and UV modulations in FO Aqu [150], the presence of accretion curtains twisted in the retrograde direction by twisted magnetic-field lines has been proposed. Similar behavior was observed in the PQ Gem system [151, 152]. Studies of the DQ Her system using eclipse mapping [153] have also indicated the presence of a twisted dipolar radiating structure near the center of the disk, suggesting the presence of twisted accretion curtains.

Investigations of the structures of the magnetic fields in the accretion disks of intermediate polars

are also of interest [154]. The magnetic field of the white dwarf can be amplified in the accretion disk by differential rotation, radial motions, and the dynamo effect. Diffusion, turbulent diffusion, and magnetic buoyancy can weaken the disk magnetic field. These effects can give rise to a magnetic field with a fairly complex structure, since different effects can dominate in different regions of the disk. The generation of toroidal magnetic field by differential rotation dominates in the inner part of the disk [155]. The character of the generated field is determined by the rotation law in the disk. However, effects associated with the presence of a poloidal velocity in the disk and redistribution of the magnetic field in the disk could also be important here [156]. The magnetic field can interact with waves arising in the inner part of the disk [128], leading to quasi-periodic variations of the rate of accretion onto the star [157]. Current sheets could form in the accretion disk [154] if the co-rotation radius exceeds the magnetosphere radius. Enhanced dissipation of the magnetic field, local increases in temperature, and radiative cooling in the UV or even X-ray will occur in these current sheets.

The complex, studies of the three-dimensional flow configurations in polars and intermediate polars require more sophisticated methods for observations and their reduction, such as Doppler tomography [122]. Three-dimensional Doppler tomography may prove preferable for studies of polars and intermediate polars [125, 126]. Observations with Spektr-UV could be used to obtain detailed two-dimensional and three-dimensional Doppler tomograms of such objects in the UV. This is especially important for studies of the physics of processes occurring in the inner parts of the accretion disks and in the region of the magnetosphere.

c. Rapidly rotating accretors. The classification of cataclysmic variables given above is universal and encompasses virtually all currently known objects of this type. However, certain systems do not fit into this classification for various reasons. The clearest example is the AE Aqr system [158]. This may be because this system is located in a super-propeller state [112], when the magnetic white dwarf is rotating extremely rapidly. The influence of the magnetic field of the rapidly rotating white dwarf on the structure of the plasma flow in its Roche lobe is so great that, instead of an accretion disk, there is an intense outflow from the system. Such white dwarfs are distinguished by a high rate of loss of their rotational energy, which is transformed into the kinetic and thermal energy of the outflowing material, and also often goes into accelerating particles in current sheets and shocks arising at the magnetosphere boundary. The spectra of super-propellers differ radically from those of accreting sources. The radiation flux is maximum in the optical and UV, but includes an additional non-thermal component associated with radiative losses by accelerated particles in and near the white-dwarf magnetosphere.

Estimates of the possible population of white dwarfs passing through a period of accretional spin-up suggest that observational searches for super-propellers in our Galaxy could be worthwhile. We currently know of only one such object, the AE Aqr system. This may be due to the fact that this system is located close to the Earth. The only means of detecting super-propellers that are at distances of more than 100 pc is to search for objects with anomalous flare activity in the optical and UV. The use of Spektr-UV observations for this purpose could be crucial.

5.2.4. Other types of interacting binary stars.

a. Binary stars interacting via their stellar winds. When the distance between the components of a binary system is large, mass transfer between them can occur via their stellar winds. Such systems include, for example, symbiotic stars [159], where one component is a giant with a high mass-loss rate via its wind and the other is a hot subdwarf or white dwarf. An accretion disk supplied by matter from the wind can form around the compact accretor in such systems. Classical symbiotic stars display flare activity (see, e.g., [160–162]) associated with non-stationary burning at the accretor surface, with the disk possibly being disrupted during flares. Studies of the flare activity of symbiotic stars can provide information about accretion onto white dwarfs and enable more detailed studies of instability of accretion disks.

The components of massive binaries such as η Carinae can also interact via their winds, forming complex flow patterns [163]. The interstellar gas can be heated to high temperatures when it passes through the shocks that form in such systems, causing it to radiate in the soft X-ray and hard UV. The UV radiation from such systems could be observed with Spektr-UV.

b. Binary Be stars. An appreciable fraction of massive B stars display emission lines in their spectra, associated with the formation of disk-like envelopes around these stars. Such stars are called Be stars, and are often binaries with white dwarfs or neutron stars as companions to the B star. The orbital periods of binary Be stars vary over a wide range from $\sim$10 to $\sim$300 days. Struve [164] hypothesized that the Be-star envelope forms from matter ejected from the rapidly rotating star by centrifugal forces. However, the rotation rates of a number of known Be stars are not sufficiently high to support this effect [165]. A model was proposed in [166] in which an outflow of matter from a star rotating at below the critical

rate came about due to the gravitational action of the secondary in a binary with the Be star. Numerical simulations carried out in [167] confirmed that this model was able to explain the observed dependence of the intensity of Be/X-star flares on their orbital periods. UV observations would make it possible to investigate the flow patterns in such stars for the first time.

c. Young binary stars. Young binary stars in the T Tauri stage are also very interesting objects. In this evolutionary stage, the components of a binary accrete the remnants of material from a protostellar cloud. This process determines a very important parameter of the future evolution—the component-mass ratio. Although the outer parts of protoplanetary disks are fairly cool and cannot be observed in the UV, the inner parts that are close to the binary components can have substantially higher temperatures.

The results of numerical simulations have shown that the flows in this region are determined by an outgoing shock that is formed by the supersonic motion of the components relative to the matter in the protoplanetary disk [168]. The interaction of these shocks with incoming matter flows also determines the ratio of the accretion rates in the system. UV observations can help determine the parameters of the outgoing shocks, which, in turn, will enable estimation of the ratio of the accretion rates and refinement of evolutionary models for these binary stars.

6. PHYSICS OF STARS, STELLAR ATMOSPHERES, AND STELLAR ACTIVITY

6.1. Evolution of Stars to the Main Sequence in the Context of the Formation of Planetary Systems and Astrochemistry

The conditions during the formation of a star determine its parameters—its mass, chemical composition, rotation rate, and, therefore, its evolution. A star's planetary system can arise and be disrupted at various times during its lifetime. A planetary system conserves the angular momentum acquired during the formation of the star. Accretion during early stages of the star's evolution gives rise to very powerful mechanisms capable of leading to the formation of optical jets and molecular outflows. The accretion energy is partially transformed into the energy of ionizing radiation, which influences the evolution of the protoplanetary disk and the subsequent formation of planets. Problems related to the nature of these mechanisms, their evolution, and their influence on the chemical evolution of the inner disk remain largely unresolved. UV observations are required for studies of the evolution of stellar atmospheres and outflows and their influence on the atmospheres of their planets.

6.1.1. Evolution of stars to the main sequence: formation of stars. The phase of evolution before the main sequence is a relatively short time interval (10^6–10^8 yrs) between the onset of gravitational compression of a gas–dust cloud and the onset of thermonuclear reactions in the core of the newly formed star. Young objects interact with the ambient medium in which they are embedded, and are characterized by a high degree of activity. They have large IR and UV excesses and very often display emission lines (see the review [169]). Additional energy is released in shocks at the surface and in gravitational–magnetic interactions between the star and disk. The kinetic energy of the incident matter goes into heating the local gas. If matter falls in along magnetic-field lines, the temperature of the gas can exceed 10^6 K [170, 171]. The X-ray emission from the shock front ionizes the incident gas, which then radiates primarily in the UV. Analysis of UV spectra can be used to deduce the accretion rate [172]. Since the density of the infalling gas is high ($n_e \simeq 10^9$–10^{12} cm^{-3}), the thickness of the radiating column is negligible compared to the radius of the star. Accretion shocks are observed as *hot spots* on the surface, and are sources of rotation-modulated emission in the visible [173] and UV [174, 175]. These observations can provide important information about the geometry of the magnetosphere and the characteristics of the accretion shock.

However, an appreciable fraction of the UV excess is not due to accretion shocks, even in sources in which rotational modulation has been detected. The stellar magnetosphere, base of the outflow, and accretion disk also contribute to the UV flux. These components of the system play a key role in transforming the gravitational energy of the gas and dust rotating in the disk into the mechanical energy of jets. The final amount of angular momentum carried from the disk to the star depends on the efficiency of this transfer on large (outflows and jets) and small (turbulence, magnetic reconnection) scales. Observations that could help elucidate the physics of these processes are few in early stages, when absorption is high; at later stages, these effects are manifest only in the UV.

Figure 8 shows that the main component of the Si III 1892 Å line cannot form in a disk wind. The theory predicts that it should be appreciably shifted, which is not observed. The dominant contribution is made by the stellar magnetosphere. Observations with Spektr-UV will provide unique opportunities to study these processes and trace the evolution of star–disk systems during the stage of planet formation.

6.1.2. Accretion and activity. A first estimate of the UV radiation can be obtained from an analysis of the ratios of the fluxes in lines corresponding to high (CIV, NV, SiIV) and low (MgII, CII, SiII) ionization stages. There is a correlation between the intensity

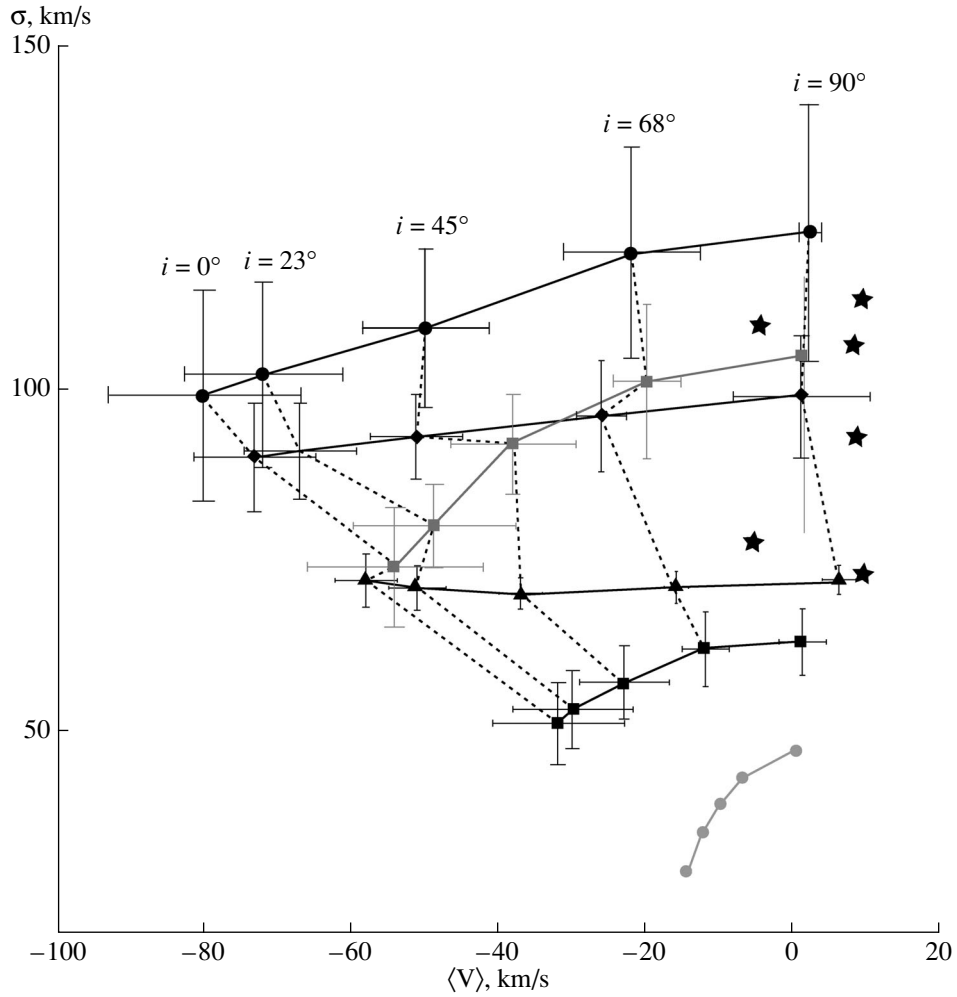

Fig. 8. Width σ of the Si III 1892 Å line as a function of the shift of the emission component $\langle V \rangle$ for various stellar-wind models (Dynamo*, Passive, Reference, Mag-2kG, and Mag-5kG) and the disk inclination i. The model values are shown by the squares. The triangles correspond to HST/STIS observations of the T Tauri stars DE Tau, AK Sco, RY Tau, RW Aur, T Tau, and RU Lup. For more detail, see [176].

of the CIV, NV, MgII, CII, and OI lines and the accretion rate [177–179]. Essentially, the accretion rates are determined from the UV excess radiated by warm matter in the accretion flow [172, 177]. The UV excess is accompanied by broadening of the UV lines. These profiles are very broad in the case of high accretion rates, and this broadening decreases as the star approaches the main sequence [179]. The UV line fluxes contain information about all the physical components of the star—its photosphere, magnetosphere, outflows (winds analogous to the solar wind), jets, accretion flows, inner disk, and remnants of gas in the young planetary system. Only analyses of high-resolution spectra at various phases of the source variability can enable separation of the contributions of the individual components [180].

6.1.3. From protoplanetary disks to planetary systems. Silicates and carbonates are important structural blocks for dust particles and planetesimals in protostellar/protoplanetary disks. The evolution of the disk depends mainly on the radiation in the far UV, which gives rise to photo-vaporization of the gaseous disk, establishing the final structure of giant planets in the system and initiating the epoch of formation of stony planets. Unfortunately, our understanding of the far UV radiation of precursors to planetary systems such as the solar system is poor. The far UV flux is probably variable in the stage preceding the main sequence. In early stages (ages of less than one million years), the protoplanetary disks are protected from hard radiation from the star. However, as young planetary disks form, they are irradiated more and more strongly by UV radiation from their very

active young stars. The strong stellar wind interacts with particles in the interplanetary medium, giving rise to diffuse helium and hydrogen emission, which permeates the young planetary system. A thousand young solar-type stars with various masses and in various stages of their pre-main-sequence evolution are located within 500 pc of the Sun. Observations of these sources with moderate spectral resolution can provide unique information about the evolution of their atmospheres, magnetospheres, and coronas, as well as their influence on the formation and evolution of planets.

The lifetime, spatial distribution, and composition of the gas and dust in young circumstellar disks (younger than 30 million years) are important characteristics for our understanding of the formation and evolution of exosolar planetary systems. The gaseous disk regulates the migration of planets [181–183], and the characteristic migration time depends on the distribution of the disk surface density and the dissipation time [184]. The formation of the cores of giant planets and the accretion of gaseous envelopes occurs on time scales close to the lifetimes of disks around T Tauri and Ae/Be Herbig stars, 10^6–10^7 yrs. UV radiation from the star effectively shapes the surface of the disk through photo-vaporization [185, 86] and determines the lifetime of the gaseous component of the disk. The time for the dust to be swept out from the disk is estimated to be two to four million years [187], but recent results have shown that the inner molecular disks in classical T Tauri stars can survive to ages of 10 million years [177, 188]. In the case of low gas densities ($<10^{-6}$ g/cm^2), fluorescent H_2 spectra in the 912–1650 Å band can be used to detect even small quantities of this gas in the protoplanetary medium. While CO spectra in the middle IR and other traditional indicators of accretion suggest dissipation of the inner gaseous disk, H_2 and CO observations in the far UV unambiguously testify to the existence of an inner ($r < 10$ AU) molecular disk [189, 190]. The penetration of UV photons to the dust disk and their energy redistribution exert a large influence on the chemical composition of the disk [191]. Photodissociation of H_2 and CO by far-UV photons controls the chemistry of the outer parts of the disk.

6.2. Active Stars

Stellar activity is manifest in the form of spots; flares; UV, X-ray, and radio emission; and various other signs. On the Sun, these phenomena are associate with strong magnetic fields, which, in turn, are generated in deep layers of the star by a dynamo process and the energy of convection, with rotation also playing a role.

Interest in stellar activity stems not only from the fact that the Sun is responsible for space weather that exerts an influence on the Earth, but also from the fact that stellar activity is part of a set of important electrodynamical processes observed everywhere in space: from the magnetospheres of planets and neutron stars to the accretion disks around T Tauri stars and Active Galactic Nuclei. Magnetic activity exerts a substantial influence on exoplanets, especially on hot Jupiters located close to their stars and on recently formed planets: the blowing away of gas by ionizing UV radiation and coronal winds of hyper-active young stars can exert a very strong influence on the chemical evolution of the outer layers of planetary atmospheres, in particular, sweeping out volatile components. This can lead to a situation where planets in the habitable zone are not fully suitable for life. (See Section 7 for more detail about prospects for exoplanet studies.)

The importance of the UV range is not only its spectral diagnostic capabilities, but also the fact that it opens possibilities for detecting motions of gas involved in active processes with high velocity resolution. This is currently not possible in the X-rays due to the huge technical difficulty in creating high-resolution spectrographs for high-energy photons. Powerful dynamics are characteristic for a wide range of phenomena associated with stellar activity: gaseous flows, explosive processes, and collimated jets. The rapid motion of the components of short-period binaries makes it possible to distinguish their spectra in velocity space. Spectra with high spectral resolution can be used to carry out Doppler mapping: distinguishing bright and dark spots on the surfaces of the rotating stars via an analysis of variations in line profiles due to variations of the projection of the velocity of a given element of a stellar surface onto the line of sight as the star rotates. An interesting aspect of measuring rotational velocities is detecting stars that are rapidly rotating, in particular, yellow giants lying in the Hertzsprung gap, which show strong broadening of the profiles of lines of highly ionized atoms, such as CIV 1548 Å, with the Doppler broadening being twice the amount expected for the rotational velocity of the star ($v \sin i$). This is explained by the presence of hot gas near the co-rotation radius of the star, at a height a factor of two higher than the level of thermal equilibrium. The question of how this gas came to be at this height remains open, although there is no doubt that this results from a balance between flare heating and cooling of gas in a system of extended magnetic loops.

Another area where UV observations can play a leading role is the so-called coronal graveyard; i.e., the very low X-ray luminosities of old red giants. This is explained by smoothing of hot magnetic structures lying beneath an extended chromosphere that has a

high optical depth in the X-ray range. Essentially, theses coronae are turned inside out compared to the solar corona: the corona is lower and the chromosphere higher. It is possible that the internal magnetic activity could play an important role in accelerating the cool winds of red giants. The mechanism of these winds is a long-standing problem in astrophysics that has a direct relationship to the chemical evolution of the Galaxy. UV spectra played an important role in searches for evidence of submerged coronal structures based on the detection of cool chromospheric absorption lines against the background of the emission of the hot coronal gas, in particular in the SiIV 1393 Å line. It is curious that analogous submerged hot structures were recently detected on the Sun: cool gas that absorbs in molecular lines is sometimes visible above hot regions radiating in the SiIV 1393, 1402 Å lines during periods of flare activity.

It is very important how the stellar spectra are measured. Experience shows that the value of UV spectra grow dramatically if they are obtained with the highest possible spectral resolution and signal-to-noise. The reason is that UV spectra carry a huge amount of information, not only about the object itself, but also about the circumstellar and interstellar media. A stellar spectrum obtained for a particular reason can be used by other researchers for a completely different aim. Thus, it is important to obtain the full UV spectrum of an object, so that it can contribute to a general spectral catalog. This observing approach using the HST/STIS made it possible to obtain high-resolution spectra for eight cool stars in 2010–2011 and for 21 hot stars in 2013–2015. These spectra were collected in the Advanced Spectral Library (ASTRAL) Project. Note that, in spite of the high UV flux, the ASTRAL program demanded observations over a large number of orbits—in all about 400. The problem is that the electronic cameras of the STIS Multi-Anode Microchannel Array (MAMA) detectors are subject to damage at high count rates. For this reason, attenuation filters were applied, increasing the exposure time required to achieve a given signal-to-noise ratio. The CCD detectors used in the WSO-UV project are more efficient in this regard, since their safe count rate limit is appreciably higher than for the STIS cameras.

6.2.1. Studies of stellar chromospheres manifesting magnetic activity using high-resolution spectroscopy. According to data obtained with the International Ultraviolet Explorer (IUE), the UV spectra of cool dwarfs manifesting chromospheric activity closely resemble the spectra of solar floccules (see, e.g., [192]). The latter are complex conglomerates of magnetic substructures that have risen from the convective layer of the Sun. Magnetic activity in these structures, such as magnetic reconnection, leads to flares and coronal mass ejections, which can sometimes accelerate electrons to relativistic speeds [193]. In spite of the fact that we cannot directly observe the surfaces of other stars, we can use the capabilities of the WSO-UV high-resolution spectrographs in the far and near UV to obtain information about the forms and arrangement of magnetic floccules in the chromospheres ($T \simeq 6000$ K), transition layers ($T \simeq 100\,000$ K), and even coronae ($T \simeq 10^6$ K) of other stars.

The Doppler mapping method discussed in Section 6 is a promising technique for obtaining information about the structure of a stellar surface [194]. Depending on the inclination of the rotation axis to the line of sight, a time series of line profiles obtained over the full rotational period of a star should enable mapping of a large fraction of its surface. Many studies of photospheric phenomena such as cool surface spots (see [194] and references therein) and related phenomena have appeared in recent decades, from the discovery of polar spots to differential rotation, migration toward poles, and even disruption rates of spots.

This method has not yet been applied to emission lines formed in the chromospheres or transition layers of stars (although first attempts have been made [195, 196]). The reason is the small number of UV photons received from cool stars, together with the need for high spectral resolution in observations of weak emission lines. Note that classical (photospheric) Doppler mapping makes the important assumption that a selected (absorption) spectral line is optically thin. This means that we cannot simply adopt and apply the photospheric Doppler-mapping method to chromospheric emission lines, such as CaII H and K-like lines, since the radiation at a given point in a line profile arrives from regions with a range of optical depths. This requires optically thin (or close to optically thin) chromospheric lines, which are located in the far and near UV. Such lines form in levels with both low (e.g., SiII 1808 Å) and high (e.g., CIV 1548 Å) excitation energies. This means that they carry information about temperature variations with depth, making it possible to establish the three-dimensional structure of the stellar atmosphere. Some UV lines (e.g., HeII 1640 Å) form in the corona. They can be included in the mapping process in order to spatially resolve weak coronal structures or check for the absence of such structures. Thus, it is hoped as part of the WSO-UV project to obtain time series of spectra with resolution $R = 50\,000$ for rapidly rotating, magnetically active stars, in which the Doppler effect should dominate over other line-broadening mechanisms.

6.2.2. Activity and magnetism of low-mass M stars. A large number of spectral lines forming in the chromospheres of stars with outer convective envelopes are located in the far and near UV. These lines are excellent indicators of stellar activity. The most valuable are lines of highly ionized atoms such as OVI, SiIV, and CIV, and the emission component of Lyα. Analysis of the profiles of these lines in high-resolution spectra with $R = 50\,000$ will provide new information about the mechanisms for energy dissipation and heating in stellar chromospheres, which will also provide links between solar and stellar physics [197].

Not only spectral lines, but also continuum fluxes are important indicators of activity and the thermal structure of the chromospheres of low-mass stars [198]. Monitoring of UV fluxes can be used to identify and trace relatively short (minutes) flare events, which is important for studies of stellar magnetic activity. Together with published magnetic-field measurements, this information can aid in constructing models for the magnetosphere and circumstellar medium in detail not previously possible. For stars with known rotational periods, the relationship between the various indicators of stellar activity and the rotational velocity will lead to a better understanding of the action of the dynamo mechanism in low-mass stars [199].

An important task in studies of activity cycles in low-mass stars is searches for variability in their UV fluxes. It is supposed that their periods should be decades, and possibly longer [200], but they have not yet been detected. The planned lifetime of the WSO-UV (Spektr-UV) mission of ~10 yrs will enable the detection of signs of activity cycles in M dwarfs. Although the level of the UV flux in these stars is low compared to their fluxes in the visible and IR, the brightest (i.e., closet) M dwarfs can be observed and studied with the intended sensitivity of the detectors.

6.3. The Origin of Heavy Elements in the Early Galaxy

Since the publication of the fundamental work of Burbidge et al. [201], it has generally been believed that elements heavier than those in the iron group (with $Z > 30$) are synthesized in neutron-capture reactions, which proceed according to either the slow (s) or rapid (r) process, depending on the flux density of neutrons. The s process in the case of nonstationary burning of a double layer source during the asymptotic-giant-branch (AGB) stage in stars of intermediate mass ($M = 1$–$4\ M_\odot$) has been best studied theoretically. A large fraction of s nuclei in solar and Galactic material were synthesized in AGB stars, and the associated process is considered to be the main s process. Some s nuclei with atomic masses $A \leq 90$ (from Ga to Zr) are produced in the weak s process in massive stars ($M > 10\ M_\odot$) in the core-helium-burning stage. There is currently no unified opinion about the astrophysical place of the r process, but it should take place in massive objects ($M > 8\ M_\odot$), such as Type II supernovae (SN II) or mergers of neutron stars, since heavy elements—europium, barium, strontium—are observed even in the oldest stars in the Galaxy that formed before the first intermediate-mass stars reached the AGB stage in their evolution and begin to enrich the interstellar medium in s nuclei. According to various estimates, this occurred at the epoch when the iron abundance in Galactic material had reached $[\mathrm{Fe/H}] = -2.5$, and possibly $[\mathrm{Fe/H}] = -1.5$.

It is natural to suppose that elements with $Z > 30$ were synthesized exclusively via the r process in stars with $[\mathrm{Fe/H}] \leq -2.5$. The contribution of the weak s process to the abundances of Ga–Zr could not be substantial, since the s process is secondary in nature, and requires the presence of seed nuclei in the medium, which are usually nuclei of iron-group elements. Indeed the observation of Ba–Hf ($56 \leq Z \leq 72$) in low-metallicity stars testifies that these nuclei arose in the r process (see the review [202]). Among the lighter elements, the best studied are Sr, Y, and Zr. Their abundances relative to iron demonstrate large scatters for stars with similar metallicities, exceeding two orders of magnitude (see [203] for a survey); at the same time, the ratios between the Sr, Y, and Zr abundances remain constant [204]. Travaglio et al. [203] proposed that some process that synthesized light elements with $30 < Z < 50$ operated in the young Galaxy, but was inefficient for heavier elements. Neither the nature of this mechanism nor the limits for its operation have been established in the theory of the chemical evolution of the Galaxy [205–207]. Resolving this problem requires observational data on the abundances of elements in the full range from Ga to Te, in order to obtain a representative sample of stars with large metal deficits.

This cannot be achieved using ground-based facilities alone. Many of the elements in this range—As, Se, Br, Kr, Cd, In, Sn, Sb, Te—do not have lines in the visible, and others (Nb, Mo, Ru, Rh) can be observed in lines of their neutral atoms, which have low ionization energies and low concentrations in stellar atmospheres, making the lines unmeasurable when $[\mathrm{Fe/H}] < -2$. The UV range, where numerous lines of both the neutral atoms and first ions of elements from Ga to Te are located, is much more informative. We have already discussed the need for observations of stars with large metal deficits as part of the WSO-UV project [208]. The idea was in the air, and such a program was proposed in 2011 for

the HST/STIS by Roederer et al. [209]. Tellurium, arsenic, and selenium were first detected in halo stars in [210. 211]. Figure 9 demonstrates the detection and quantitative analysis of the SeI 2039.85 Å and GeI 2041.71 Å lines in a spectrum obtained with $R \simeq 110\,000$ on HST/STIS (http://archive.stsci.edu), for the halo star HD 140283 (program GO-7348). The range from Ga to Te has been most fully studied for two stars—HD 108317 and BD +17°3248 [212]. This includes 17 elements, for 7 of which data were available only from UV spectra.

The statistics for determining elemental abundances from UV spectra are still low, and it is not yet possible to establish trends in the behavior of the elemental-abundance ratios, which could shed light on sources of chemical enrichment of the Galactic material in early stages of the Galaxy. Spektr-UV (WSO-UV) can make a considerable contribution to resolving this problem through observations of stars with metal deficits at wavelengths 2000–3000 Å with high-resolution spectrographs ($R \simeq 50\,000$).

6.4. Stratification of Elements in the Atmospheres of Chemically Peculiar (Ap) Stars

The peculiar chemical composition of the atmospheres of magnetic Ap stars has been explained using the theory of the diffusive separation of elements [213]. The effect of the stratification of elements on UV spectral-line profiles has been discussed earlier in studies dedicated to the WSO-UV project [208, 214]. Mainly, iron-group elements and rare-earth elements in the atmospheres of cool regions of Ap stars were considered, where a sharp jump in the abundances of these elements with depth is observed (see, e.g., [215] for Pr). Analysis of stratification requires observed line profiles for elements in various ionization stages. For iron-peak elements, these are lines of the neutral elements, as well as the first, and sometimes second, ionization stages; for rare-earth elements, these are lines of the first and second ionization stages. Virtually all the rare-earth elements are observed in lines of the first ionization stage in the visible, but only some of these elements—Ce, Pr, Nd, Tb, Dy—have strong enough lines in the second ionization stage. Lines of LaIII, EuIII, GdIII, TmIII, YbIII, and LuIII are mainly located in the UV at wavelengths shorter than 3000 Å. Therefore, detailed studies of the distribution of as large a number of rare-earth elements as possible in the atmospheres of Ap stars require high-accuracy UV spectral observations.

Computations of the diffusion of elements in stellar atmospheres hotter than 10 000 K [216] show substantial differences of the distribution with depth compared to cooler stars with $T_{\rm eff} = 8000$ K. For example, for the four iron-peak elements Ti, Cr, Fe, and Ni, the theory predicts higher excesses at the formation depths of most of the lines, without the presence of appreciable gradients. Analysis of the chemical composition of the Ap star HD 170973 with $T_{\rm eff} = 11\,200$ K indicates a good agreement between the observed profiles for lines of these four iron-peak elements with theoretical profiles calculated using diffusion models [217]. The abundances of these elements determined using usual methods without stratification applied to spectra at wavelengths 3100–10 000 Å coincide with the theoretical values at the formation depths of the spectral lines obtained using diffusion models within the uncertainties [217]. However, the abundances of the odd iron-peak elements Sc, V, Mn, and Co predicted by the diffusion theory turn out to be substantially higher than is obtained from a usual analysis of the chemical composition using visible spectra. The same picture is observed for lighter elements, such as Mg. The Mg abundances determined using usual methods applied to lines of neutral and ionized Mg in the visible differ by 0.4 dex, and both values are substantially lower than is predicted by the diffusion theory. Figure 10 shows a comparison of synthetic spectra in the region of the MgII UV doublet calculated for the diffusion model and for a model with the same atmospheric parameters but with an abundance corresponding to observations in the visible. Spectral UV observations of Ap stars with various temperatures will undoubtedly help refine the diffusion computations for individual elements.

6.5. UV Spectroscopy of White-Dwarf Precursors with Hydrogen Deficits

The final stage in the evolution of stars of low and intermediate masses begins with their departure from the AGB. They evolve with constant luminosity to extremely high effective temperatures ($T_{\rm eff} > 100\,000$ K), with hydrogen and helium burning in layer sources. When nuclear burning has ceased, the evolutionary track of the star moves to the hot edge of the white-dwarf cooling sequence. The standard theory of post-AGB evolution predicts that the chemical composition at the stellar surface remains rich in hydrogen, because the burning in layer sources ceases when the hydrogen-rich surface layer and region rich in helium are reduced to masses of $10^{-4}\ M_\odot$ and $10^{-2}\ M_\odot$, respectively. This scenario, which leads to the formation of hydrogen-rich white dwarfs, operates for most post-AGB stars. However, a significant fraction of such stars do not follow this path. Roughly 25% of post-AGB stars with planetary nebulae and

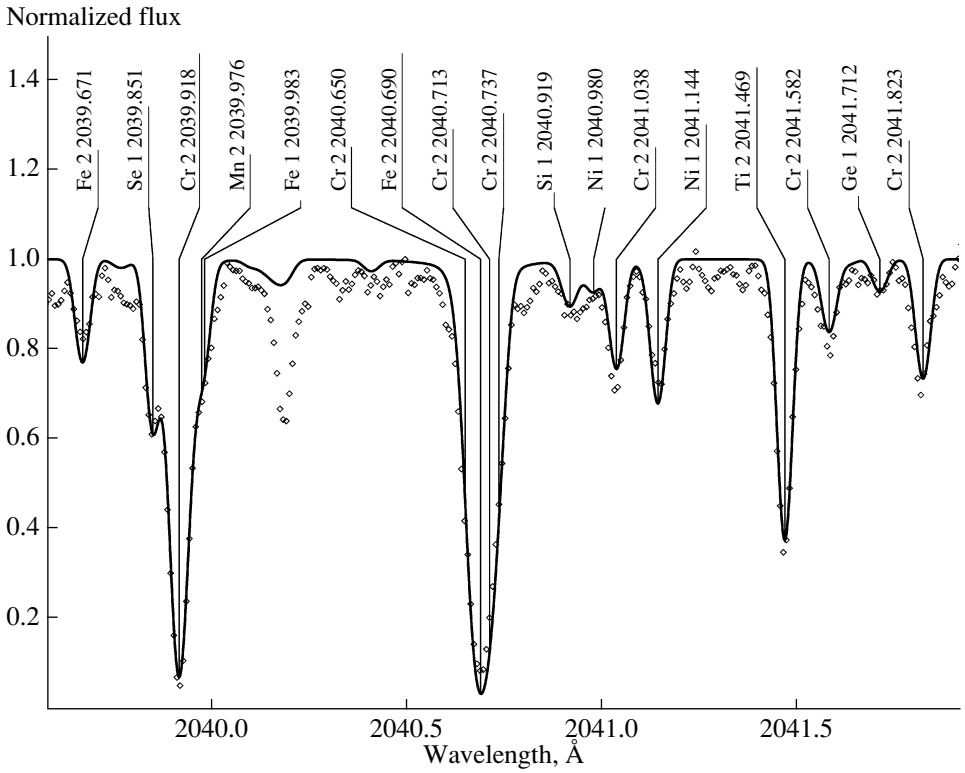

Fig. 9. SeI 2039 Å and GeI 2041.71 Å lines in the spectrum of HD 140283 (diamonds) and a theoretical spectrum calculated for a model atmosphere with $T_{\rm eff} = 5780$ K, $\log g = 3.70$, [Fe/H] $= -2.46$ and the abundances [Se/Fe] $= -0.86$ and [Ge/Fe] $= -0.60$ (solid curve). Identifications for the strongest lines are indicated.

with white-dwarf precursors display a deficit of hydrogen. An example of such stars is the "evolutionary sequence" Wolf–Rayet star (WC), PG 1159 star, and helium-rich white dwarf (DO) with $T_{\rm eff} = 70\,000$ K.

The atmospheres of WC stars and PG 1159 stars consist mainly of He, C, and O (usually, He comprises 30%, C 50%, and O 20% by mass). This strange composition confirms the hypothesis [218] that the origin of the hydrogen-poor post-AGB sequence is a late episode of helium burning. Under certain conditions, burning in a He layer source is ignited in a white dwarf. The star returns to the AGB (it is a "reborn" AGB star), and passes through its post-AGB evolution a second time. The ignition of the helium gives rise to mixing and burning of the remaining surface hydrogen. Material from deep layers (the region between the H and He layer sources) is exhausted at the surface. Well known examples of such "reborn" stars are FG Sge and Sakurai's object.

As a consequence of mixing due to the helium ignition, iron-group elements (i.e., elements with atomic numbers $z > 28$) synthesized in the stellar precursors to the AGB stars and accumulated in the inter-layer region should exhibit strong abundance excesses in the atmospheres of WC and PG 1159 stars, and also in the hottest DO white dwarfs. While these elements have not been detected in WC and PG 1159 stars, they have been detected in hot DO white dwarfs.

RE 0503−289 is a hot DO white dwarf with $T_{\rm eff} = 70\,000$ K, $\log g = 7.5$. It has a fairly high carbon abundance (about 5% by mass), which is substantially higher than is typical for other DO dwarfs (<1%), but much lower than the carbon abundance of PG 1159 stars (10–60%). A far-UV spectrum of this star was obtained with the FUSE observatory. Rauch et al. [219] and Werner et al. [220] detected lines of highly ionized elements beyond the iron peak in these spectra. Excesses were found for a number of elements (Zn, Ga, Ge, Kr, Xe, Ba), from 155 to 23 000 times the solar abundances.

Is the object RE 0503−289 unique? It is tempting to suspect that, like PG 1159 stars, the UV spectra of other DO dwarfs will contain lines of elements beyond the iron peak. Thus, UV spectroscopy provides unique opportunities to directly investigate the results of nucleosynthesis via neutron capture (the *s* process).

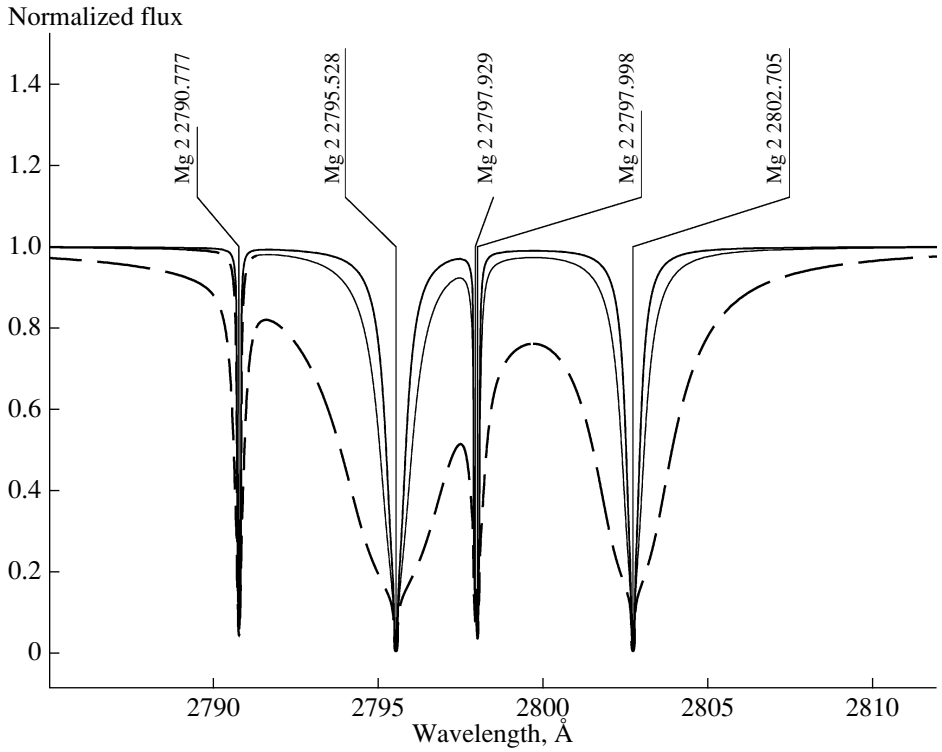

Fig. 10. Comparison of synthetic spectra in the region of the MgII UV doublet calculated for the parameters of the Ap star HD 170973 ($T_{\rm eff} = 11\,000$ K). The solid and dot-dashed curves show the spectra calculated using the Mg abundances obtained from MgI lines and MgII lines in the visible, respectively, and the dashed curve the spectrum calculated using a diffusion model.

6.6. Hot Subdwarfs in the UV

The Hertzsprung–Russell diagram displays the main sequence, corresponding to stars in the stage of core hydrogen burning, from low-mass red stars to massive blue stars, and also the regions of red giants, hot supergiants, and white dwarfs. Less well known are a group of very blue stars lying to the left of the main sequence. They are too weak to be main-sequence stars, but too bright to be white dwarfs. These are low-luminosity O and B stars—sdO and sdB subdwarfs, which are the most numerous blue ($U - B < -0.4$) population in the sky among stars brighter than $m_V = 18^m$. Normal subdwarfs are low-mass ($\sim 0.5\ M_\odot$) stars in the helium-burning stage with a thin hydrogen envelope and hydrogen-rich atmosphere; they are sometimes described as extreme horizontal-branch stars [221]. The universal nature of their structure hides their varied properties and evolutionary origin, which is related to fairly extreme physical conditions in the stellar cores. In many cases, determining the nature of sdO and sdB subdwarfs requires UV spectroscopy.

In the case of effective temperatures between 25 000 and 45 000 K, a large fraction of the flux is emitted and absorbed in the UV. The atmospheres of most subdwarfs have non-standard chemical composition; their chemical stratification is due to radiative pressure and diffusion acting on individual ions. There is a deficit of helium and other light elements, and excesses of elements heavier than calcium, apart from iron. Fewer than 20 subdwarfs have been studied in detail in the UV, where metals determine the spectral energy distribution. Diagnostics of surface temperature, surface gravity, and chemical composition based on observations in the visible are only as good as the model atmospheres that are used with them, which must be tested using UV observations, especially for the most chemically peculiar objects.

Appreciable (to 2 dex) excesses of lead, germanium, and zirconium have been measured for normal sdB stars using UV spectra [222, 223]. In the case of sdB stars enriched in heavy elements, the excesses for Zr, Ge, Sr, Y, and Pb measured using several lines in the visible were 4 dex [224, 225]. The influence of this peculiar chemical composition on the UV spectra and the entire structure of the atmosphere has not yet been established, for either normal or extreme subdwarfs.

Low-amplitude, multi-mode surface pulsations have been detected for hot subdwarfs. Approximately every tenth subdwarf with $T_{\rm eff} = 30\,000$–$35\,000$ K

demonstrates p-mode pulsations with periods from 2–10 min. Roughly half such stars with $T_{\rm eff} = 25\,000$–$30\,000$ K display g-mode pulsations with periods from one to two hours. A significant number of subdwarfs have been observed with the Kepler Space Observatory [226]. Astroseismological observations can be used to accurately determine the masses and internal structures of hot subdwarfs. A key parameter of astroseismological studies is the effective temperature, which is determined spectroscopically, making UV observations important. Furthermore, the UV plays an important role in the identification of the pulsation models for sdB stars, since the amplitude of the modes is maximum in the UV. This makes it possible to use the pulsations to directly estimate the radius.

The UV range is important for studies of the role of hot subdwarfs in old stellar populations, in order to use them as cosmochronometers. Since higher spatial resolution can be achieved in the UV than at longer wavelengths, this provides the best means for detecting relatively rare hot subdwarfs in globular clusters, to determine whether they differ from field subdwarfs [227]. It is very important to obtain and analyze UV spectra for subdwarfs in several globular clusters. The UV excesses of giant elliptical galaxies is related to the number of hot subdwarfs. Their existence means that some time had passed since the formation of the galaxy, and the metallicity had reached some level. Consequently, the number of subdwarfs is an indicator of the age of a galaxy [228–230]. It is of interest to carry out deep surveys of galaxies with UV excesses, in order to investigate how these indicators are related to the mass and metallicity of the galaxy, and therefore to study the evolution of stars in various ambient conditions and at various epochs.

6.7. Physics of Supernovae

It is clear from general considerations that extending the observed spectral range by adding UV data should enhance the reliability of derived parameters of supernovae based on modeling of optical photometric and spectroscopic data. However, we will limit our consideration to questions for which spectral observations in the UV could make a decisive contribution.

6.7.1. Initial peak of the luminosity of Type IIP supernovae. Type IIP supernovae (SN IIP) result from the explosion of a red supergiant with an initial mass exceeding 9 $M_\odot$. Light curves together with spectral data make it possible in the framework of radiative gas dynamics to derive the main parameters of the supernova: its mass, the energy of the explosion, and the radius of the pre-supernova. The explosion energy and mass of the star on the main sequence are very important phenomenological parameters for the theory of the collapse and explosion of massive stars. With the increase in the number of well studied supernova in recent years, the serious problem arose that masses derived in different ways did not coincide: as a rule, the masses of the pre-supernovae found from hydrodynamical modeling were a factor of 1.5 higher than mass estimates based on photometry of the pre-supernovae from archival images of their host galaxies [231, 232]. Attempts to remove this contradiction have thus far been unsuccessful.

A perspective method for testing the reliability with which SN IIP parameters are determined is modeling the initial luminosity peak with a duration of about a week. Since the luminosity, temperature, and velocity at the photospheric level at this stage depend substantially on the radius of the pre-supernova, modeling the initial luminosity peak would make it possible to estimate the radius of the pre-supernova with high accuracy. In turn, fixing the radius of the pre-supernova provides the possibility of finding more reliable estimates of the mass and energy via hydrodynamical modeling of the total light curve taking into account spectral data. It is possible that this will help resolve the problem of the disagreement between different mass estimates.

Obtaining a detailed picture of the behavior of the initial luminosity peak requires observations in both the visible and the UV, since the temperature substantially exceeds 10^4 K at the early stage. To successfully derive the pre-supernova radius, it is desirable to obtain a series of at least three low-resolution UV spectra, for example, one, two, and five days after the emergence of the shock at the surface. For SN IIP of moderate luminosity at the stage $t = 2$ days, the model luminosity is $\approx 4 \times 10^{42}$ erg/s [231], the photospheric radius 1.7×10^{14} cm, and the temperature 2×10^4 K. At a distance of 20 Mpc, the 2500 Å flux at the Earth would be 9×10^{-14} erg cm^{-2} s^{-1} Å^{-1}. Observations with HST/STIS spectograph (G230L grating, $R = 500$) would require five seconds in order to obtain a spectrum with a signal-to-noise ratio $S/N = 10$ at 2500 Å. The exposure would have to be twice as long for a spectral resolution of 1000.

6.7.2. Superluminous supernovae. Recently, based on data from the PTF survey, Quimby et al. [233] distinguished a class of supernova with colossal luminosities—so-called "superluminous supernovae" (SLSN). Their luminosities are $\sim(2$–$3) \times 10^{44}$ erg/s at the brightness maximum at about 40–50 days. The energy source for SLSN is unknown. Two mechanisms are popular: a magnetar mechanism and accretion onto a black hole. SLSN are rare events, corresponding to about one per 10^4 massive-star collapses. For this reason, SLSN have been detected only at redshifts 0.2–1.5. The spectra of

SLSN close to the maximum brightness are blue, with their peak flux near 3000 Å. Their spectral lines are unusual for supernovae: only absorption lines of O II at wavelengths 3600–4600 Å are present in the visible; an intense Mg II absorption line and other absorption features that are identified with lines of Si III and C II can be distinguished at the short UV wavelengths of 1500–2500 Å [233]. There are no lines of hydrogen or helium. It is most likely that the pre-supernova is the carbon–oxygen core of a massive star.

The UV spectra of SLSN carry important information about the expansion velocity at the photospheric stage and the chemical composition of the envelope. UV spectra of SLSN at high redshifts $z > 0.5$ can be observed with large ground-based telescopes. Obtaining UV spectra at small redshifts requires extra-atmospheric observations. Let us consider as an example the event LSQ14bdq, with redshift $z = 0.35$ [234]. Nineteen days before the maximum, the flux at 3000 Å was 2×10^{-16} erg cm^{-2} s^{-1} Å^{-1}. Observations with HST/STIS (G230L grating, $R = 500$) would require 5700 s in order to obtain a spectrum with $S/N = 10$. With a spectral resolution of 1000, the exposure time required for the same signal-to-noise ratio would be 12 000 s.

6.7.3. Outer envelope of the Crab Nebula. The Crab Nebula with its pulsar is the most studied young (≈1000 yrs) Type IIP supernova remnant. However, it is not clear to what extent this supernova was a standard SN IIP. According to the estimates of [235], the kinetic energy of the explosion giving rise to the Crab Nebula was $\sim 3 \times 10^{49}$ erg. This is one and a half orders of magnitude lower than for normal SN IIP, and an order of magnitude lower than for SN 2003Z, which had a low explosion energy [236]. The observed radial velocities of the optical filaments in the Crab Nebula lie within an interval of 1500 km/s [235], which is appreciably below the characteristic expansion velocities of SN IIP envelopes, which are $3100(E_{51}/M_{10})^{1/2}$ km/s, where E_{51} is the kinetic energy in units of 10^{51} erg and M_{10} is the mass of the envelope in units of 10 $M_\odot$. The velocity of the outer layers of an SNe IIP envelope is even higher, $\approx 10^4$ km/s.

The problem of the anomalously low energy of the Crab Nebula can be solved in a natural way if we suppose that there is some invisible material (an "outer envelope") with a higher expansion velocity beyond the filamentary nebula. The kinetic energy of the outer envelope could appreciably exceed estimates of the energy of the Crab Nebula, thus removing the energy-deficit problem. The presence of an outer envelope does not contradict observations. Indeed, the visible nebula is formed by the interaction of relativistic plasma from the thermalized pulsar wind with inner layers of the supernova envelope. This leads to the formation of a network of filaments with a huge density contrast, of order $\sim 10^3$ relative to the mean density. This why the inner, excited part of the envelope is clearly visible, while the outer, unperturbed envelope is not.

Lundqvist et al. [237] proposed observing the outer envelope in resonance lines of Li-like ions of CNO elements in absorption against the background of the pulsar radiation. Sollerman et al. [238] realized this idea using HST/STIS with the G140L grating ($R = 1000$) in order to obtain spectra of the pulsar in the Crab Nebula at 1140–1720 Å. The resulting spectrum obtained with an exposure time of 14 000 s shows signs of an outer envelope: absorption in lines of the C IV 1548, 1551 Å doublet in the radial-velocity interval from −2500 to −1200 km/s (Fig. 11). The low signal-to-noise ratio prevents establishing the detailed behavior of the radial concentration of C IV. Estimating the mass and energy of the outer envelope based on the C IV absorption requires absorption spectra in this range with high signal-to-noise ratios (preferably 20). This can be achieved with the long-slit spectrograph on the WSO-UV.

A higher-quality C IV 1550 Å absorption spectrum will yield data on the distribution of the C IV density over a wide range of velocities. Using an ionization model, these data can be used to derive the mass and kinetic energy of the envelope, and thus determine whether the supernova of 1054 is a normal SN IIP. In any case, with the derived energy and mass, the Crab Nebula would turn out to be the only known Type II supernova remnant with a normal pulsar. This would be very important for our understanding of the explosion mechanism for SN IIP and the genesis of pulsars. Note that the neutron stars associated with two known Type II supernovae with normal explosion energies (SN 1987A and Cas A) do not show signs of pulsar activity.

6.8. Precise Determination of the Sources of UV Continuum Absorption as a Means to Improve Modeling of Stellar Atmospheres and Spectral Synthesis

The development of important areas of modern astrophysics, such as studies of the chemical properties of various populations in our Galaxy, planetary systems, etc., led to a return to the question of the accuracy with which the parameters of stars are determined (their temperature, surface gravity, and chemical composition), from first principles. An accuracy of several percent can be achieved for objects

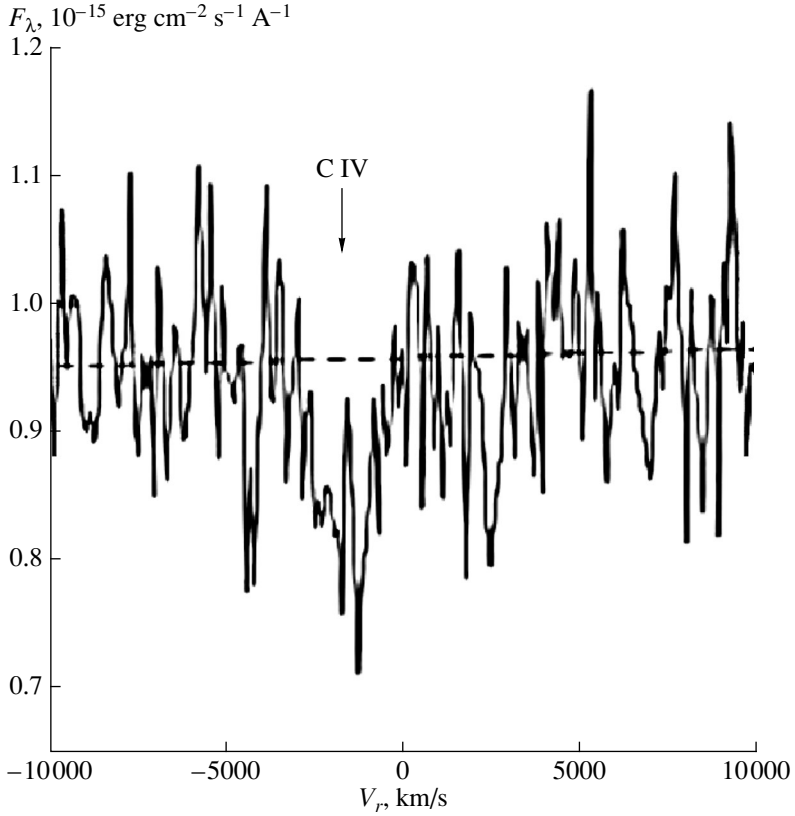

Fig. 11. C IV 1550 Å absorption spectrum toward the Crab pulsar obtained on the HST with the STIS [238]. The CIV 1550 Å absorption in the interval of radial velocities from −2500 to −1200 km/s indicates the presence of gas with high velocities in the outer envelope of the Crab Nebula.

with similar parameters, in the case of a differential analysis; however, this accuracy is rapidly lost when the stars being compared are appreciably different. In the case of cool stars (from M to F), the "guilt" for uncertainties in the atmospheric parameters is usually ascribed to the quality of atomic data, deviations from LTE, incorrect account of convection in the atmosphere, and incomplete allowance for sources of continuum absorption. Considerable attention has already been paid to the first three factors. For example, projects such as VALD3 and VAMDC have cardinally improved the quality and completeness of atomic and molecular data. Efforts aimed at taking into account deviations from LTE led to the creation of models for atoms that are able to correctly calculate level populations. Efforts to construct three-dimensional hydrodynamical models of stellar atmospheres have met with success. The accuracy of the parameters determined was improved, but the desired level of 5% was not reached. A project directed at studying the completeness of known sources of continuum absorption, verifying the accuracy of computed cross sections, modernizing modeling of stellar atmospheres, and detailed spectral analyses is needed. Inadequate description of continuum absorption not only changes the structure of the model, but also influences the depths of spectral lines, which are the main source of information on stellar parameters. The most dramatic deviations are observed in the UV, where the contribution of metals is comparable to or larger than the contribution of hydrogen and helium. Figure 12 illustrates this effect for the star α Cen A. the theory satisfactorily reproduces the observations in the cores of strong lines, but there are considerable discrepancies in the wings. The idea of the project is to obtain high-accuracy ($S/N > 150$) spectra of a series of bright main-sequence stars. All the objects have angular-diameter measurements with accuracy no worse than 5%. the UV spectroscopy will be supplemented by archival ESO and NASA data in the visible. Specialists on atomic physics will be involved in order to perfect the computations of absorption cross sections. Systematic measurements of UV spectra of stars in the temperature interval from 4500 to 7000 K with various chemical compositions will enable the determination the origin discrepancies and refine existing and add missing continuum absorption cross sections. This will make it possible to remove

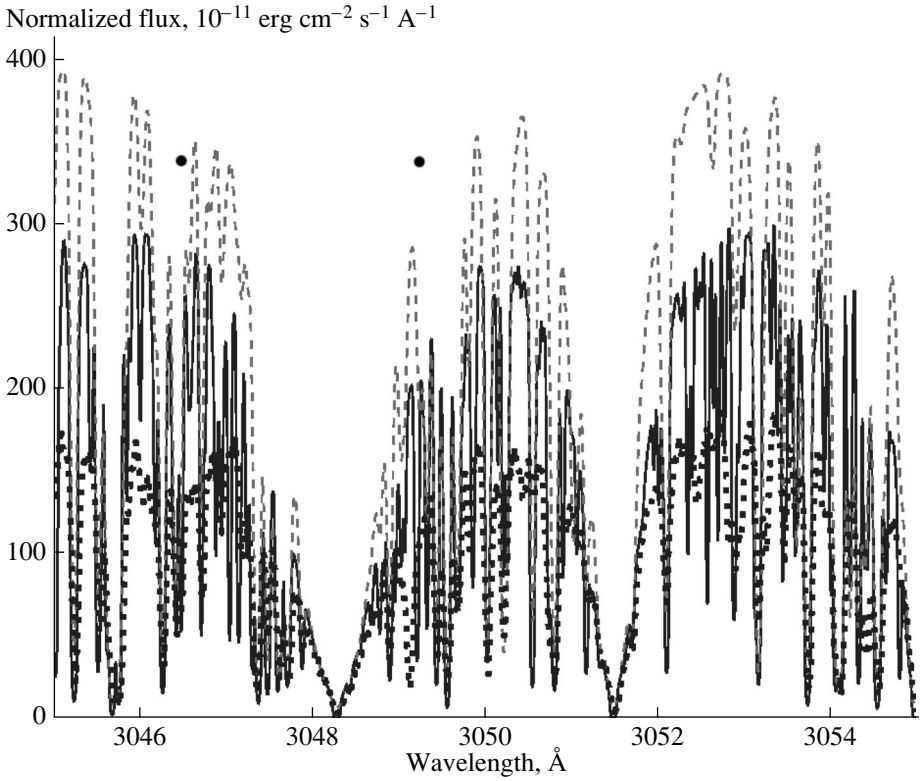

Fig. 12. Spectrum of the star α Cen A obtained with HST/STIS (bold points) compared to theoretical spectra calculated using the SME (dashed curve) and Phoenix (solid curve) programs.

one of a number of difficulties remaining on the path to determining high-accuracy stellar parameters.

7. PLANETARY ATMOSPHERES

In our solar system, and also in other planetary systems, a whole series of objects could be perspective targets for observations with Spektr-UV. Most resonance lines of atoms and fluorescent transitions of simple ions and molecules are located in the UV, and this is where the dissociation and ionization of most atmospheric molecules and atoms by photons of solar (or stellar) radiation occur. We do not propose to present a detailed description of all possible observational tasks here, and limit our consideration to a fairly narrow set of themes for which UV observations with Spektr-UV could make a fundamental contribution.

7.1. Atmospheres of Planets and Small Bodies in the Solar System

The modern theory of planetary exospheres is based primary on the results of space observations of their characteristic emission properties in atomic lines such as the hydrogen Lα 121.6 nm and Lβ 102.6 nm lines, the helium 58.4 nm line, and the oxygen 130.4 and 135.6 nm lines. Observations of planetary atmospheres from space have been carried out since the beginning of the space era, making it possible to improve data on complex processes in the outer layers of planetary atmospheres. It follows from the data obtained that upper planetary atmospheres are populated both with a fraction of thermal atoms with mean kinetic energies corresponding to the exosphere temperature and a fraction of hot atoms with mean kinetic energies much higher than the exosphere temperature. The fraction of suprathermal (hot) particles is formed in non-thermal processes initiated by the action of solar UV radiation and the solar-wind plasma on the atmosphere. These processes are accompanied by an intense transfer of energy between various degrees of freedom of the atmospheric particles and the substantial thermal effect of photochemical reactions. The resulting observational manifestations of hot atoms confirmed theoretical predictions of the important role of non-equilibrium processes involving suprathermal particles in planetary atmospheres [239]. A new direction in planetary aeronomy is currently being actively developed: investigation of the role of suprathermal particles in the physics and chemistry of planetary

atmospheres [239–241]. It follows from the most important results of such studies that suprathermal (hot) particles in excited states forming in the upper layers of atmospheres give rise to non-thermal atmospheric emission and enhance non-thermal atmospheric losses, thereby determining the evolution of the atmosphere on astronomical time scales. Studies of UV line emission from bodies in the solar system and extrasolar planetary systems taking into account the suprathermal characteristics of the medium are of fundamental importance.

7.1.1. UV emission by water vapor in the solar system. Searches for water, in particular, emission by water vapor in the UV, and theoretical interpretation of such emission, is a fundamental direction in studies of space physics and chemistry. Small bodies such as asteroids, comets, and interplanetary dust, which are important components of the solar system and which physically and evolutionarily interact closely with large planets, are of special interest. The resolution of fundamental questions concerning the origin and evolution of the solar system and the origin of life are directly related to these bodies, whose matter has undergone minimal variation in the course of its evolution.

The dissociation of water vapor in gaseous envelopes surrounding small bodies by solar UV radiation and/or fluxes of high-energy ions and electrons is a multi-channel process; the formation of OH molecules in electronically excited states begins with the absorption of photons with wavelengths shorter than 137 nm, and the formation of O atoms with the absorption of photons with wavelengths shorter than 177 nm. Note that the dissociation products can form as suprathermal particles, whose energies usually appreciably exceed the thermal energy of the surrounding atmospheric gas. Further, O atoms and OH molecules in metastable ^{1}D, ^{1}S, and $A^2\Sigma^+$ states can either emit photons in the transitions $\mathrm{OH}(A^2\Sigma^+ \rightarrow X^2\Pi,\ \lambda = 305, 325$ nm), $\mathrm{O}(^1S \rightarrow {}^3P_{0,1,2},\ \lambda = 295.8,\ 297.2$ nm), $\mathrm{O}(^1S \rightarrow {}^1D,\ \lambda =$ 557.7 nm), and $\mathrm{O}(^1D \rightarrow {}^3P_{0,1,2},\ \lambda = 630,\ 636.2$ nm), or be quenched in collisions with ambient atmospheric particles. For example, water molecules are vaporized from the surface of a cometary nucleus due to heating by solar radiation. The molecules that are ejected into the coma are dissociated into molecular fragments under the action of solar photons and can become ionized. The main component of cometary nuclei—water molecules—is manifest in the coma as atoms of H and O and OH radicals. All three types of particle have very strong transitions in the UV, where these three types of emission can be simultaneously detected with high spatial resolution [242]. Other parent molecules, such as CO and CO_2, can also be studied through their UV line emission. For example, HST observations of the intensities of UV emission from H and O in the region near the south pole of Jupiter's moon Europa and Saturn's moon Enceladus, where ejections of water vapor had been noted, were recently carried out [243]. These data are considered to provide additional evidence for the existence of water oceans beneath the icy surfaces of moons and the possible astrobiological potential of such moons.

7.1.2. UV emission of H, C, N, and O from planetary atmospheres. The composition of the upper atmospheres of planets is determined to a large extent through analyses of UV spectral observations. The upper atmospheres of planets are predominantly populated by atoms of H, C, N, and O [240]. High-spectral-resolution UV observations of the H and O lines Lα 121.6 nm, OI 130.4 nm, and OI 135.6 nm in the atmospheres of planets have shown that the formation of the profiles of these emission lines is governed by both thermal and non-thermal processes in the uppermost layers of the atmospheres. The detailed analysis [240] of HST observations of a number of atomic emission lines in the upper atmospheres of the terrestrial planets and Jupiter and the near-surface atmospheres of Europa and Enceladus indicate contributions from both thermal and suprathermal atoms in excited states.

Observations and analysis of UV line emission will enable studies of the kinetics of the formation and collisional relaxation of thermal and suprathermal atoms of H, N, C, and O, as well as water molecules, in the upper atmospheres of terrestrial planets. Joint observations with space-based UV spectral observations will also enable estimation of the current dissipation rates of atmospheres.

7.1.3. Auroral phenomena in the UV. Charged particles moving along magnetic-field lines of planets give rise to auroral phenomena (the Earth, Jupiter, Saturn). Recent observations with the IUVS spectrometer on the MAVEN spacecraft have now also confirmed the existence of polar aurora on Mars [244]. Extreme solar events—powerful flares, coronal ejections of plasma, etc.—are important factors reflecting the influence of the Sun on the states of planetary atmospheres, and can affect variations in climate. Studies of perturbations in the magnetosphere–ionosphere systems of planets due to extreme solar events, which are manifest as polar aurora, are of special interest. The brightness, spectrum, structure, and geometrical form of polar aurora are directly dependent on the characteristics of the fluxes of electrons and protons of magnetospheric and solar (stellar) origin that are incident on the ionosphere, which give rise to the complex dynamics of the resulting physical and chemical processes. The polar

atmospheres of planets in the solar system is precisely where such solar–planetary links are manifest most intensely.

One of the most important manifestation of these interactions is UV line emission from the atmosphere in polar aurorae, caused by the penetration of electrons, protons, and H atoms with high kinetic energies into the atmosphere. For example, the Lα emission has two components: a very strong component—located exactly at the line center at 121.5667 nm, from the cool planetary corona, and a weaker Doppler-shifted emission component from H atoms forming during the recharging of protons incident onto the polar upper atmosphere in collisions with atoms and molecules of the ambient atmosphere.

The brightest UV line in polar aurorae in the atmospheres of terrestrial planets is emission from atomic O at 130.4 nm. However, this emission is strongly scattered in the atmosphere, making it difficult to obtain the distribution of the intensities of the sources created as a result of the arrival of particles with high kinetic energies. The emission in the O 135.6 nm line is less scattered by the atmosphere, making it an excellent characteristic for visualization of polar aurora. Thus, an important requirement for measurements is the ability to detect and spectrally distinguish the emission at 135.6 nm and 130.4 nm. Comparison of the emission intensities at the shortest and longest UV wavelengths can be used to obtain a parameter that can be related to the height of the emission peak, and accordingly with the energy of the incident electrons. Inverting the relationship between the various emission lines makes it possible to obtain the mean energy and flux of the incident electrons [245].

Diagnostic UV emission from H_2 could be used to monitor the precipitation of magnetospheric electrons with high kinetic energies over the entire disk of a giant planet, with a special accent on the polar regions. An analysis of spectral UV observations of the polar regions of Jupiter obtained with HST/STIS was recently reported in [246]. These observations were used to construct the first spectral maps of polar aurorae on Jupiter in the UV. Future observations with Spektr-UV will make possible detailed studies of specific regions of polar aurorae.

We should note the complex of mathematical models for the calibration and interpretation of UV images of polar aurorae, developed earlier and refined using Monte Carlo models [247–252]. These enable joint analyses of processes related to the precipitation of electrons, protons, and H atoms with high kinetic energies into the polar regions of a planetary atmosphere. During the NASA IMAGE (studies of the Earth's magnetosphere), ESA Mars-Express, and ESA Venus-Express projects, these models for the kinetics of suprathermal particles in excited states were used to calculate synthetic emission lines for the calibration of UV instruments and interpretation of the results of UV observations of lines in the atmospheres of terrestrial planets [251, 253].

8. UV LINE EMISSION FROM THE ATMOSPHERES OF EXOPLANETS

Observations of extrasolar planets using ground and space telescopes in the IR and UV will enable the first estimates of important characteristics of the atmospheres of objects of various mass in extrasolar planetary systems, such as their chemical composition and thermal state.

The exoplanets known as hot Jupiters are currently being intensely studied. These are massive gas giants (with masses comparable to the mass of Jupiter) located in the immediate vicinity of their stars (at distances from their stars of no more than 0.1 AU), giving rise to intense processes and facilitating their detection. Observations of hot Jupiters using the HST testify to complex physical processes in the gaseous envelopes (atmospheres) of these planets. For example, the absorption in the Lα line for the exoplanet HD 209458b as it transits its star reaches 9–15% [254–256]. At the same time, the disk of the planet reduces the brightness of the star by 1.8% due to eclipsing. This means that the planet is surrounded by an extensive envelope of neutral hydrogen that extends beyond its Roche lobe. This was later confirmed by transit observations in lines of C, O, and Si [257–259]. The depth of the transit in these lines reaches 8–9%. Two main hypotheses have been put forth to explain the existence of this envelope. The first is the expansion of the planetary atmosphere due to heating by radiation from the star [260, 261], which gives rise to outflows of matter at rates of $\sim 10^{10}$ g/s. The second is based on the mechanism of charge-exchange of ions in the stellar wind during collisions with atoms in the atmosphere [262]. The atoms that are formed have sufficiently high energies to leave the gravitational field of the planet, enabling them to form an envelope around the planet.

Currently, detailed, careful studies of only three hot Jupiters have been carried out in the UV, namely HD209458b, HD189733b, and WASP-12b. A general result obtained from analysis of the UV observations for these three planets is the presence of an extended, evaporating upper atmosphere [254, 263]. This so-called hydrodynamical outflow of atmosphere is established when the incident soft X-ray and EUV flux from the central star is sufficiently strong to appreciably heat the upper atmosphere of

the planet [260, 264, 265]. As a result, the atmosphere begins to dynamically expand, pushing the upper atmosphere beyond the Roche lobe or the magnetosphere protecting the atmosphere from the stellar wind [266], leading to mass loss from the atmosphere [267]. Heavy atoms (such as C, O, Mg, and Fe [257, 259, 263, 268, 269]) have also been detected in the exospheres of these planets, demonstrating that heavy elements present in lower layers of the atmosphere can be captured when they evaporate into the exosphere. Atmospheric evaporation is the only and main common denominator of observations acquired thus far, and models predict that many planets in close orbits should be subject to this process.

Moreover, observations of these hot giant planets have enabled the discovery of another interesting phenomenon—lacks of coincidence of the beginning or end of the transits in different wavelength ranges. This was first detected by Fossati et al. [263] in 2009 in HST UV observations of a transit of WASP-12b, carried out in several bands with widths of 40 Å. According to these data, the beginning of the transit in some light curves leads the beginning of the transit in the visible by approximately 50 min, testifying to the presence of absorbing material located ahead of the planet at a distance of roughly four to five planetary radii. Bisikalo et al. [270] proposed that the earlier eclipse could arise due to the formation of a closed, aspherical envelope around WASP-12b, whose size substantially exceeds the limits of its Roche lobe.

Understanding details of the evaporation process is important for constructing a picture of the formation of planets and distributions of their parameters. For example, high mass-loss rates suggest the existence of a population of planets with low masses and nearly no atmospheres (such as CoRoT-7b and Kepler-10b) for which detections will grow in the future, some of which could be remnant cores of vaporized planets with masses comparable to that of Neptune [267, 271].

Spektr-UV is considered to be an effective means to study mechanisms for the vaporization of upper layers of the atmospheres (exospheres) of exoplanets. UV spectral observations during transits of a sufficiently large set of exoplanets in close orbits with various characteristics will provide the best opportunities for studying the vaporization of planetary atmospheres. Analysis of transit light curves obtained in selected UV lines can be used to estimate the temperature, pressure, and dynamical structure in the upper layers of exoplanet atmospheres.

The characteristics of the central stars and their influence on their exoplanets is currently weakly studied, and UV observations of planetary transits will also provide important data on stellar activity, which exerts a substantial influence on the evolution of planets [272]. UV observations of transits of planets in close orbits will also give unique opportunities to estimate the physical properties of the stellar wind (its temperature, density, velocity, etc.), especially in the important transition region where the wind is accelerated. Such information is currently known only for the Sun (see, e.g., [273]).

The evolution of the atmospheres and possible habitability of planets are related—in early stages of the evolution of planetary systems, planets in the habitable zone will undergo expansion of their thermospheres. As a result, vaporization is a key process when estimating the possible habitability of planets revolving around their stars in the habitable zone [274]. Therefore, UV observations will provide the possibility of estimating and placing limits on numerous models for the evolution of planets and their atmospheres currently used to study potential habitability. Thus, UV observations of transits of Earth-like exoplanets around Sun-like stars using Spektr-UV (WSO-UV) will present unique opportunities for shedding light on the early evolution of Earth-like planets, including those in our solar system [275].

9. CONCLUSION

Ultraviolet astronomy is an important and rapidly developing area of studies of the Universe. The results of the successful in-orbit operation of missions such as IUE, ASTRON, the Hubble Space Telescope, FUSE, and GALEX convincingly confirm the high importance of UV observations for the development of modern astrophysics. Unfortunately, there are no next-generation UV projects planned by major space agencies that would be realized before 2030. For the first time in many decades of space research, the problem arose of access of the astronomical community to UV observations, which will become more serious after the end of the functioning of the HST. The major international project World Space Observatory—Ultraviolet planned for the period 2021–2030 is essentially the main and only means of providing access to UV observations until the launch of next-generation missions.

ACKNOWLEDGMENTS

We thank G.S. Bisnovatyi-Kogan, B.V. Komberg, A.S. Pozanenko, and K.A. Postnov for useful discussions.

This work was supported by the Russian Foundation for Basic Research (grants 13-02-00642, 14-29-06059, 14-02-00215, 14-02-00838a, 15-02-06365, and 15-02-08476a) and the Basic Research Program

of the Presidium of the Russian Academy of Sciences (P-9 and P-41).

The study of D.V. Bisikalo and V.I. Shematovich was supported by the Russian Science Foundation (project no. 15-12-300038).

REFERENCES

1. E. I. Moskalenko, *Methods of Extra-Atmospheric Astronomy* (Nauka, Moscow, 1984) [in Russian].
2. V. E. Panchuk, M. V. Yushkin, and B. M. Shustov, J. Opt. Technol. **73**, 256 (2006).
3. V. Shustov, M. Sachkov, A. I. Gomez de Castro, K. Werner, N. Kappelmann, and A. Moisheev, Astrophys. Space Sci. **335**, 273 (2011).
4. M. E. Sachkov, Vestn. FGUP NPO S.A. Lavochkina **3**, 16 (2013).
5. *Fundamental Space Research,* Vol. 1: *Astrophysics,* Ed. by G. G. Raikunov (FGUP TsNIImash, Korolev, 2013) [in Russian].
6. N. Brosch, V. Balabanov, and E. Behar, Astrophys. Space Sci. **354**, 205 (2014).
7. J. B. Hutchings, Astrophys. Space Sci. **354**, 143 (2014).
8. S. Martin, in *Proceedings of the 40th Scientific Assembly of the Committee on Space Research COSPAR* (2014), p. 2013.
9. P. Côté, Adv. Space Res. **53**, 982 (2014).
10. C. Neiner, P. Petit, L. Parès, and Parès, in *Magnetic Fields throughout Stellar Evolution,* IAU Symp. **302**, 348 (2014); arXive:1311.2264.
11. S. R. Heap, J. W. Kruk, J. R. Rigby, and M. Robberto, in *Abstracts of the 221st American Astronomical Society Meeting* (2013), 147.27.
12. P. A. Scowen and H. SDT, in *Abstracts of the 221st American Astronomical Society Meeting* (2013), 439.04.
13. D. N. Spergel, J. Kasdin, R. Belikov, P. Atcheson, M. Beasley, D. Calzetti, B. Cameron, C. Copi, S. Desch, and A. Dressier, Bull. Am. Astron. Soc. **41**, 362 (2009).
14. B. A. Pasquale, P. Stahl, L. Feinberg, J. Howard, Q. Gong, and D. Aronstein, SPIE Conf. Ser. **7731**, 2 (2010).
15. A. I. Gómez de Castro, T. Appourchaux, M. A. Barstow, M. Barthelemy, F. Baudin, S. Benetti, P. Blay, N. Brosch, E. Bunce, D. de Martino, J.-M. Deharveng, R. Ferlet, K. France, M. García, B. Gänsicke, et al., Astrophys. Space Sci. **354**, 229 (2014); arXiv:1306.3358.
16. T. Raksasataya, A.-I. Gómez de Castro, L. Koechlin, and J.-P. Rivet, Exp. Astron. **30**, 183 (2011).
17. B. Shustov, M. Sachkov, A. I. Gómez de Castro, K. Werner, N. Kappelmann, and A. Moisheev, Astrophys. Space Sci. **335**, 273 (2011).
18. M. E. Sachkov, B. M. Shustov, A. A. Moisheev, and O. V. Vlasenko, Vestn. FGUP NPO S.A. Lavochkina **5**, 34 (2014).
19. M. Sachkov, V. Shustov, I. Savanov, and A. I. Gómez de Castro, Astron. Nachr. **335**, 46 (2014). doi:10.1002/asna.201312015
20. B. M. Shustov, M. E. Sachkov, A. A. Boyarchuk, A. A. Moisheev, and A. I. Gomez de Kastro, Vestn. FGUP NPO S.A. Lavochkina **5**, 4 (2014).
21. V. G. Zhupanov, V. N. Fedoseev, E. A. Golyshko, and A. A. Moisheev, Vestn. FGUP NPO S.A. Lavochkina **5**, 92 (2014).
22. V. Panchuk, M. Yushkin, T. Fatkhullin, and M. Sachkov, Astrophys. pace Sci. **354**, 163 (2014).
23. A. S. Shugarov, I. S. Savanov, and S. Kuzin, Vestn. FGUP NPO S.A. Lavochkina **5**, 86 (2014).
24. J. A. Kolhneier, D. H. Weinberg, V. D. Oppenheimer, F. Haardt, N. Katz, R. Davé, M. Fardal, P. Madau, S. Danforth, A. B. Ford, M. S. Peeples, and J. McEwen, Astrophys. J. **32**, 789 (2014).
25. V. Khare and R. Srianand, Mon. Not. R. Astron. Soc. **451**, L30 (2015).
26. A. S. G. Robotham and S. P. Driver, Month. Not. R. Astron. Soc. **413**, 2570 (2011).
27. P. Madau and M. Dickinson, Ann. Rev. Astron. Astrophys. **52**, 415 (2014).
28. S. P. Driver, P. D. Allen, and J. Liske, Astrophys. J. **657**, L85 (2007).
29. M. Fukugita, S. J. Hogan, and P. J. E. Peebles, Astrophys. J. **503**, 518 (1998); astro-ph/9712020.
30. M. Fukugita and P. J. E. Peebles, Astrophys. J. **616**, 643 (2004); astro-ph/0406095.
31. M. E. Anderson and J. N. Bregman, Astrophys. J. **714**, 320 (2010); arXiv:1003.3273.
32. M. McQuinn, Astrophys. J. Lett. **780**, L33 (2014); arXiv: 1309.4451.
33. M. Pettini, in *Chemical Evolution from Zero to High Redshift,* Ed. by J. R. Walsh and M. R. Rosa (1999), p. 233, astro-ph/9902173.
34. A. Ferrara, E. Scannapieco, and J. Bergeron, Astrophys. J. Lett. **634**, L37 (2005), astro-ph/0510525.
35. J. H. Knapen, T. J. Mahoney, and A. Vazdekis, Eds., *Pathways through an Eclectic Universe,* ASP Conf. Ser. **390** (2008).
36. Yu. A. Shchekipov, B. M. Shustov, E. O. Vasil'ev, and S. Yu. Dedikov, in *Ultraviolet Universe II,* Ed. by B. M. Shustov, M. E. Sachkov, and E. Yu. Kil'pio (Yanus, Moscow, 2008), p. 229 [in Russian].
37. S. Campana, R. Salvaterra, A. Ferrara, and A. Pallottini, Astron. Astrophys. **575**, A43 (2015); arXiv:1501.00913.
38. K. Nandra, D. Barret, X. Barcons, A. Fabian, J.-W. den Herder, L. Piro, M. Watson, C. Adami, J. Aird, J. M. Afonso, D. Alexander, C. Argiroffi, L. Amati, M. Arnaud, J.-L. Atteia, et al., arXiv:1306.2307 (2013).
39. T. Ohashi, Y. Ishisaki, Y. Ezoe, S. Yamada, S. Yamaguchi, N. Miyazaki, Y. Tawara, K. Mitsuda, N. Y. Yamasaki, Y. Takei, K. Sakai, K. Nagayoshi, R. Yamamoto, A. Chiba, and T. Hayashi, arXiv:1503.08405 (2015).
40. O. Y. Gnedin, L. Hernquist, and J. P. Ostriker, Astrophys. J. **514**, 109 (1999).
41. J. N. Bregman, Ann. Rev. Astron. Astrophys. **45**, 221 (2007), 0706.1787.
42. J. M. Shull, B. D. Smith, and C. W. Danforth, Astrophys. J. **759**, 23 (2012), 1112.2706.

43. R. A. Simcoe, W. L. W. Sargent, M. Rauch, and G. Becker, Astrophys. J. **637**, 648 (2006); astro-ph/0508116.
44. J. Tumlinson, C. Thorn, J. K. Werk, J. X. Prochaska, T. M. Tripp, D. H. Weinberg, M. S. Peeples, J. M. O'Meara, B. D. Oppenheimer, J. D. Meiring, N. S. Katz, R. Davé, A. B. Ford, and K. R. Sembach, Science **334**, 948 (2011); arXiv:1111.3980.
45. S. Mathur, F. Nicastro, and R. Williams, in *Astrophysics in the Far Ultraviolet: Five Years of Discovery with FUSE,* Ed. by G. Sonneborn, H. W. Moos, and B.-G. Andersson, ASP Conf. Ser. **348**, 354 (2006).
46. C. W. Danforth, J. T. Stocke, B. A. Keeney, S. V. Penton, J. M. Shull, Y. Yao, and J. C. Green, Astrophys. J. **743**, 18 (2011).
47. F. Nicastro, M. Elvis, Y. Krongold, S. Mathur, A. Gupta, C. Danforth, X. Barcons, S. Borgani, E. Branchini, R. Cen, R. Davé, J. Kaastra, F. Paerels, L. Piro, J. M. Shull, Y. Takei, and L. Zappacosta, Astrophys. J. **769**, 90 (2013); arXiv:1210.7177.
48. S. Yu. Dedikov and Yu. A. Shchekinov, Astron. Rep. **48**, 9 (2004).
49. J. Schaye, R. F. Carswell, and T.-S. Kim, Mon. Not. R. Astron. Soc. **379**, 1169 (2007); astro-ph/0701761.
50. M. de Avillez and M.-M. Mas-Low, Astrophys. J. **581**, 1047 (2002).
51. N. G. Bochkarev, E. A. Karitskaya, V. V. Shimansky, and G. A. Galazutdinov, Astron. Nachr. **334**, 835 (2012).
52. J. Scab and B. G. Elmegreen, Ann. Rev. Astron. Astrophys. **42**, 275 (2004).
53. S. Yu. Dedikov and Yu. A. Shchekinov, Astron. Rep. **48**, 9 (2004).
54. E. O. Vasiliev, S. Yu. Dedikov, and Yu. A. Shchekinov, Astrophys. Bull. **64**, 317 (2009).
55. J. L. Pineda, W. D. Langer, T. Velusamy, and P. F. Goldsmith, Astron. Astrophys. **554**, 103 (2013).
56. Yu. A. Shchekinov, Astrophysics **47**, 205 (2004).
57. C. Heiles, Astrophys. J. **481**, 193 (1997)
58. S. Stanimirović, J. M. Weisberg, Z. Pei, K. Tuttle, and J. T. Green, Astrophys. J. **720**, 415 (2010)
59. P. Dutta, J. N. Chengalur, N. Roy, W. M. Goss, M. Arjunwadkar, A. H. Minter, C. L. Brogan, and T. J. W. Lazio, Month. Not. R. Astron. Soc. **442**, 647 (2014)
60. M. A. Walker, in *Small Ionized and Neutral Structures in the Diffuse Interstellar Medium,* ASP Conf. Ser. **365**, 299 (2007)
61. C. R. Gwin, Yu. Y. Kovalev, M. D. Johnson, and V. A. Soglasnov, Astrophys. J. Lett. **794**, L14 (2015).
62. J. Armstrong, B. J. Rickett, and S. R. Spangler, Astrophys. J. **443**, 209 (1995).
63. B. Godard, E. Falgarone, and G. Pineau des Forêts, Astron. Astrophys. **570**, A27 (2014).
64. T. P. Snow, T. L. Ross, J. D. Destree, M. M. Drosback, A. G. Jensen, B. L. Rachford, P. Sonnentrucker, and R. Ferlet, Astrophys. J. **688**, 1124 (2008).
65. E. B. Burgh, K. France, and E. B. Jenkins, Astrophys. J. **708**, 334 (2010).
66. T.-H. Lim, K.-W. Min, and K.-I. Seon, Astrophys. J. **765**, 107 (2013).
67. Y.-S. Jo, K.-W. Min, K.-I. Seon, J. Edelstein, and W. Han, Astrophys. J. **738**, 91 (2011).
68. E. B. Jenkins, Astrophys. J. **700**, 1299 (2009).
69. N. V. Voshchinnikov and T. Henning, Astron. Astrophys. **517**, A45 (2010).
70. T. P. Stecher, Astrophys. J. **142**, 1683 (1965).
71. E. L. Fitzpatrick and D. Massa, Astrophys. J. **663**, 320 (2007).
72. L. A. Valencic, G. C. Clayton, and K. D. Gordon, Astrophys. J. **616**, 912 (2004).
73. N. V. Voshchinnikov, T. Henning, M. S. Prokopjeva, and H. K. Das, Astron. Astrophys. **541**, A52 (2012).
74. N. V. Voshchinnikov and H. Hirashita, Mon. Not. R. Astron. Soc. **445**, 301 (2014).
75. G. A. Shields, Nature **272**, 706 (1978).
76. I. Hubeny, O. Blaes, J. H. Krolik, and E. Agol, Astrophys. J. **559**, 680 (2001); astro-ph/0105507.
77. N. I. Shakura and R. A. Sunyaev, Astron. Astrophys. **24**, 337 (1973).
78. I. D. Novikov and K. S. Thorne, in *Black Holes (Les Astres Occlus),* Ed. by C. Dewitt and B. S. Dewitt (Gordon and Breach, New York, 1973), p. 343.
79. A. Lawrence, Mon. Not. R. Astron. Soc. **423**, 451 (2012), 1110.0854.
80. E. W. Bonning, G. A. Shields, A. C. Stevens, and S. Salviander, Astrophys. J. **770**, 30 (2013); arXiv:1210.6997.
81. A. Laor and S. W. Davis, Mon. Not. R. Astron. Soc. **438**, 3024 (2014), 1312.3556.
82. P. Abolmasov and N. I. Shakura, Mon. Not. R. Astron. Soc. **427**, 1867 (2012), 1208.1678.
83. A. Khokhlov, I. D. Novikov, and C. J. Pethick, Astrophys. J. **418**, 181 (1993).
84. R.-F. Shen and C. D. Matzner, Astrophys. J. **784**, 87 (2014); arXiv:1305.5570.
85. S. Komossa, J. High Energ. Phys. (2015, in press).
86. P. V. Ivanov and M. A. Chernyakova, Astron. Astrophys. **448**, 843 (2006); astro-ph/0509853.
87. B. V. Komberg, Sov. Astron. **11**, 727 (1968).
88. M. C. Begelman, R. D. Blandford, and M. J. Rees, Nature **287**, 307 (1980).
89. L. P. Grishchuk, V. M. Lipunov, K. A. Postnov, M. E. Prokhorov, and B. S. Sat'yaprakash, Phys. Usp. **44**, 1 (2001).
90. R. V. Ivanov, J. S. V. Papaloizou, and A. G. Polnarev, Mon. Not. R. Astron. Soc. **307**, 79 (1999); astro-ph/9812198.
91. P. B. Ivanov, I. V. Igumenshchev, and I. D. Novikov, Astrophys. J. **507**, 131 (1998).
92. P. B. Ivanov, J. C. B. Papaloizou, S.-J. Paardekooper, and A. G. Polnarev, Astron. Astrophys. **576**, A29 (2015); arXiv: 1410.3250.
93. S. Roedig, J. H. Krolik, and M. S. Miller, Astrophys. J. **785**, 115 (2014); arXiv:1402.7098.

94. M. J. Valtonen, H. J. Lehto, K. Nilsson, J. Heidt, L. O. Takalo, A. Sillanpää, C. Villforth, M. Kidger, G. Poyner, T. Pursimo, S. Zola, J.-H. Wu, X. Zhou, K. Sadakane, M. Drozdz, et al., Nature **452**, 851 (2008); arXiv:0809.1280.
95. M. J. Graham, S. G. Djorgovski, D. Stern, E. Glikman, A. J. Drake, A. A. Mahabal, C. Donalek, S. Larson, and E. Christensen, Nature **518**, 74 (2015); arXiv:1501.01375.
96. T. Liu, S. Gezari, S. Heinis, E. A. Magnier, W. S. Burgett, K. Chambers, H. Flewelling, M. Huber, K. W. Hodapp, N. Kaiser, R.-P. Kudritzki, J. L. Tonry, R. J. Wainscoat, and C. Waters, Astrophys. J. Lett. **803**, L16 (2015); arXiv:1503.02083.
97. T. A. Boroson and T. R. Lauer, Nature **458**, 53 (2009), 0901.3779.
98. J. Poutanen, G. Lipunova, S. Fabrika, A. G. Butkevich, and P. Abolmasov, Mon. Not. R. Astron. Soc. **377**, 1187 (2007), astro-ph/0609274.
99. S. Fabrika, Astrophys. Space Phys. Rev. **12**, 1 (2004); astro-ph/0603390.
100. A. Vinokurov, S. Fabrika, and K. Atapin, Astrophys. Bull. **68**, 139 (2013); arXiv:1302.5630.
101. Y. Hui, J. H. Krolik, and I. Hubeny, Astrophys. J. **625**, 913 (2005); astro-ph/0502355.
102. P. Abolmasov, S. Fabrika, O. Sholukhova, and V. Afanasiev, Astrophys. Bull. **62**, 36 (2007); astro-ph/0612765.
103. S. M. Caballero-Nieves, D. R. Gies, S. T. Bolton, P. Hadrava, A. Herrero, T. S. Hillwig, S. B. Howell, W. Huang, L. Kaper, P. Koubský, and M. V. McSwain, Astrophys. J. **701**, 1895 (2009), 0907.2422.
104. K. O'Brien, K. Home, R. I. Hynes, W. Chen, S. A. Haswell, and M. D. Still, Mon. Not. R. Astron. Soc. **334**, 426 (2002); astro-ph/0204018.
105. S. D. Vrtilek, W. Penninx, J. S. Raymond, F. Verbunt, P. Hertz, K. Wood, W. H. G. Lewin, and K. Mitsuda, Astrophys. J. **376**, 278 (1991).
106. A. M. Cherepashchuk, *Close Binary Systems* (Fizmatlit, Moscow, 2013), Vols. 1, 2 [in Russian].
107. S. H. Lubow and F. H. Shu, Astrophys. J. **198**, 383 (1975).
108. A. Yu. Sytov, P. V. Kaigorodov, D. V. Bisikalo, O. A. Kuznetsov, and A. A. Boyarchuk, Astron. Rep. **51**, 836 (2007).
109. A. Yu. Sytov, D. V. Bisikalo, P. V. Kaigorodov, and A. A. Boyarchuk, Astron. Rep. **53**, 428 (2009).
110. A. A. Boyarchuk, D. V. Bisikalo, O. A. Kuznetsov, and V. M. Chechetkin, *Mass Transfer in Close Binary Stars* (Taylor and Francis, London, 2002).
111. A. M. Fridman and D. V. Bisikalo, Phys. Usp. **51**, 551 (2008).
112. A. G. Zhilkin, D. V. Bisikalo, and A. A. Boyarchuk, Phys. Usp. **55**, 115 (2012).
113. D. V. Bisikalo, A. G. Zhilkin, and A. A. Boyarchuk, *Gas Dynamics of Close Binary Stars* (Fizmatlit, Moscow, 2013) [in Russian].
114. A. Shugarov, I. Savanov, M. Sachkov, P. Jerram, I. Moody, P. Pool, P. Turner, R. Pittock, S. Kuzin, and N. Waltham, Astrophys. Space Sci. **354**, 169 (2014).
115. D. M. Townsley and L. Bildsten, in *Proceedings of the 15th European Workshop on White Dwarfs,* Ed. by R. Napiwotzki and M. R. Burleigh, ASP Conf. Ser. **372**, 557 (2007).
116. L. G. Althaus, A. H. Córsico, J. Isern, and E. García-Berro, Astron. Astrophys. Rev. **18**, 471 (2010); arXiv:1007.2659.
117. A. H. Córsico and L. G. Althaus, Astron. Astrophys. **569**, A106 (2014); arXiv:1408.6708.
118. D. V. Bisikalo and A. G. Zhilkin, in *IAU Symp. No. 282: From Interacting Binaries to Exoplanets: Essential Modeling Tools,* Ed. by M. T. Richards and I. Hubeny (Cambridge Univ. Press, Cambridge, 2012), p. 509.
119. M. Kato and I. Iben, Jr., Astrophys. J. Lett. **394**, L47 (1992).
120. I. Hachisu, M. Kato, and K. Nomoto, Astrophys. J. Lett. **470**, L97 (1996).
121. H. S. Stockman, G. D. Schmidt, J. Liebert, and J. B. Holberg, Astrophys. J. **430**, 323 (1994).
122. T. R. Marsh and K. Horne, Mon. Not. R. Astron. Soc. **235**, 269 (1988).
123. D. A. Kononov, P. V. Kaigorodov, D. V. Bisikalo, A. A. Boyarchuk, M. I. Agafonov, O. I. Sharova, A. Yu. Sytov, and D. Boneva, Astron. Rep. **52**, 835 (2008).
124. D. Boneva, P. V. Kaigorodov, D. V. Bisikalo, and D. A. Kononov, Astron. Rep. **53**, 1004 (2009).
125. M. I. Agafonov and O. I. Sharova, Astron. Nachr. **326**, 143 (2005).
126. D. A. Kononov, M. I. Agafonov, O. I. Sharova, D. V. Bisikalo, A. G. Zhilkin, and M. Yu. Sidorov, Astron. Rep. **58**, 881 (2014).
127. V. W. Borges and R. Baptista, Rev. Mex. Astron. Astrofis. Conf. Ser. **26**, 167 (2006).
128. D. V. Bisikalo, A. A. Boyarchuk, P. V. Kaigorodov, O. A. Kuznetsov, and T. Matsuda, Astron. Rep. **48**, 449 (2004).
129. V. S. Dhillon, D. A. Smith, and T. R. Marsh, Mon. Not. R. Astron. Soc. **428**, 3559 (2013); arXiv:1210.7145.
130. E. P. Kurbatov, D. V. Bisikalo, and P. V. Kaigorodov, Phys. Usp. **57**, 787 (2014).
131. R. G. Izzard, P. D. Hall, T. M. Tauris, and S. A. Tout, in *IAU Symp. No. 283: Planetary Nebulae: An Eye to the Future,* Ed. by A. Manchado, L. Stanghellini, and D. Schönberner (Cambridge University Press, 2012), p. 95.
132. G. T. Bath, Nature Phys. Sci. **246**, 84 (1973).
133. M. A. Abramowicz, X. Chen, S. Kato, J.-P. Lasota, and O. Regev, Astrophys. J. Lett. **438**, L37 (1995); astro-ph/9409018.
134. P. Godon, E. M. Sion, F. Cheng, B. T. Gänsicke, S. Howell, S. Knigge, W. M. Sparks, and S. Stanfield, Astrophys. J. **602**, 336 (2004); astro-ph/0310876.
135. M. Cropper, Space Sci. Rev. **54**, 195 (1990).

136. A. J. Norton, G. A. Wynn, and R. V. Somerscales, Astrophys. J. **614**, 349 (2004); astro-ph/0406363.
137. J. Patterson, Publ. Astron. Soc. Pacif. **106**, 209 (1994).
138. G. D. Schmidt, S. S. West, J. Liebert, R. F. Green, and H. S. Stockman, Astrophys. J. **309**, 218 (1986).
139. S. M. A. Meggitt and D. T. Wickramasinghe, Mon. Not. R. Astron. Soc. **236**, 31 (1989).
140. K. Wu and D. T. Wickramasinghe, in *Vina del Mar Workshop on Cataclysmic Variable Stars,* Ed. by N. Vogt, ASP Conf. Ser. **29**, 203 (1992).
141. F. Euchner, S. Jordan, K. Beuermann, K. Reinsch, and V. T. Gansicke, Astron. Astrophys. **451**, 671 (2006); astro-ph/0602112.
142. K. Beuermann, F. Euchner, K. Reinsch, S. Jordan, and V. T. Gansicke, Astron. Astrophys. **463**, 647 (2007); astro-ph/0610804.
143. P. A. Mason, I. L. Andronov, S. V. Kolesnikov, E. P. Pavlenko, and M. Shakovskoy, in *Cape Workshop on Magnetic Cataclysmic Variables,* Ed. by D. A. H. Buckley and B. Warner, ASP Conf. Ser. **85**, 496 (1995).
144. A. D. Schwope, H.-C. Thomas, K. Beuermann, V. Burwitz, S. Jordan, and R. Haefner, Astron. Astrophys. **293**, 764 (1995).
145. A. G. Zhilkin, D. V. Bisikalo, and P. A. Mason, Astron. Rep. **56**, 257 (2012).
146. D. V. Bisikalo, A. G. Zhilkin, P. V. Kaigorodov, V. A. Ustyugov, and M. M. Montgomery, Astron. Rep. **57**, 327 (2013).
147. P. Rodríguez-Gil and S. V. Potter, Mon. Not. R. Astron. Soc. **342**, LI (2003); astro-ph/0303144.
148. P. Rodríguez-Gil and M. A. P. Torres, Astron. Astrophys. **431**, 289 (2005); astro-ph/0410348.
149. P. A. Evans, S. Hellier, G. Ramsay, and M. Cropper, Mon. Not. R. Astron. Soc. **349**, 715 (2004); astro-ph/0312379.
150. K. O. Mason, Mon. Not. R. Astron. Soc. **285**, 493 (1997).
151. S. B. Potter, M. Cropper, K. O. Mason, J. H. Hough, and J. A. Bailey, Mon. Not. R. Astron. Soc. **285**, 82 (1997).
152. R. K. Saito, R. Baptista, K. Home, and P. Marten, Astron. J. **139**, 2542 (2010); arXiv:1005.1612.
153. P. E. Boynton, L. M. Crosa, and J. E. Deeter, Astrophys. J. **237**, 169 (1980).
154. A. G. Zhilkin and D. V. Bisikalo, Astron. Rep. **54**, 840 (2010).
155. *Magnetohydrodynamics in Binary Stars,* Ed. by S. G. Campbell, Vol. 216 of *Astrophysics and Space Science Library* (Kluwer, Dordrecht, 1997).
156. G. S. Bisnovatyi-Kogan and A. A. Ruzmaikin, Astrophys. Space Sci. **42**, 401 (1976).
157. A. G. Zhilkin and D. V. Bisikalo, Adv. Space Res. **45**, 437 (2010).
158. H. P. Ikhsanov and N. G. Beskrovnaya, Astron. Rep. **56**, 589 (2012).
159. A. A. Boyarchuk, in *The Realm of Interacting Binary Stars,* Ed. by J. Sahade, G. E. McCluskey, Jr., and Y. Kondo, Vol. 177 of *Astrophysics and Space Science Library* (Kluwer, Dordrecht, 1993), p. 189.
160. E. Kilpio, D. Bisikalo, N. Tomov, and M. Tomova, Astrophys. Space Sci. **335**, 155 (2011).
161. N. A. Tomov, M. T. Tomova, and D. V. Bisikalo, in *Proceedings of the 4th School and Workshop on Space Plasma Physics,* Ed. by I. Zhelyazkov and T. M. Mishonov, AIP Conf. Proc. **1551**, 30 (2013); arXiv:1301.2762.
162. N. A. Tomov, M. T. Tomova, and D. V. Bisikalo, Astron. Nachr. **335**, 178 (2014).
163. T. I. Madura, T. R. Gull, A. T. Okazaki, S. M. P. Russell, S. P. Owocki, J. H. Groh, M. F. Corcoran, K. Hamaguchi, and M. Teodoro, Mon. Not. R. Astron. Soc. **436**, 3820 (2013); arXiv:1310.0487.
164. O. Struve, Astrophys. J. **73**, 94 (1931).
165. J. M. Porter, Mon. Not. R. Astron. Soc. **280**, L31 (1996).
166. P. Harmanec, D. V. Bisikalo, A. A. Boyarchuk, and O. A. Kuznetsov, Astron. Astrophys. **396**, 937 (2002).
167. P. V. Kaigorodov and D. V. Bisikalo, Astron. Rep. **56**, 945 (2012).
168. A. M. Fateeva, D. V. Bisikalo, P. V. Kaygorodov, and A. Y. Sytov, Astrophys. Space Sci. **335**, 125 (2011).
169. T. D. Oswalt and M. A. Barstow, *Planets, Stars and Stellar Systems,* Vol. 4: *Stellar Structure and Evolution* (Springer, Dordrecht, 2013).
170. S. Lamzin, Astron. Rep. **42**, 322 (1998).
171. E. Gullbring, L. Hartmann, C. Briceno, and N. Calvet, Astrophys. J. **492**, 323 (1998).
172. L. Ingleby, N. Calvet, G. Herczeg, A. Blaty, F. Walter, D. Ardila, R. Alexander, S. Edwards, C. Espaillat, S. G. Gregory, L. Hillenbrand, and A. Brown, Astrophys. J. **767**, 112 (2013); arXiv:1303.0769.
173. J. Bouvier, K. N. Grankin, S. H. P. Alencar, C. Dougados, M. Fernández, G. Basri, C. Batalha, E. Guenther, M. A. Ibrahimov, T. Y. Magakian, S. Y. Melnikov, P. P. Petrov, M. V. Rud, and M. R Zapatero Osorio, Astron. Astrophys. **409**, 169 (2003); astro-ph/0306551.
174. T. Simon, F. J. Vrba, and W. Herbst, Astron. J. **100**, 1957 (1990).
175. A. I. Gómez de Castro and M. Fernandez, Mon. Not. R. Astron. Soc. **283**, 55 (1996).
176. A. I. Gómez de Castro and B. von Rekowski, Mon. Not. R. Astron. Soc. **411**, 849 (2011); arXiv:1011.1230.
177. L. Ingleby, N. Calvet, E. Bergin, G. Herczeg, A. Brown, R. Alexander, S. Edwards, C. Espaillat, K. France, S. G. Gregory, L. Hillenbrand, E. Roueff, J. Valenti, F. Walter, C. Johns-Krull, et al., Astrophys. J. **743**, 105 (2011); arXiv:1110.6312.
178. A. I. Gómez de Castro and P. Marcos-Arenal, Astrophys. J. **749**, 190 (2012).
179. A. I. Gómez de Castro, Astrophys. J. **775**, 131 (2013), 1306.3338.
180. A. I. Gómez de Castro and S. A. Lamzin, Astrophys. Space Sci. **335**, 61 (2011).

181. W. R. Ward, Astrophys. J. Lett. **482**, L211 (1997).
182. P. J. Armitage, M. Livio, S. H. Lubow, and J. E. Pringle, Mon. Not. R. Astron. Soc. **334**, 248 (2002); astro-ph/0204001.
183. D. E. Trilling, J. I. Lunine, and W. Benz, Astron. Astrophys. **394**, 241 (2002); astro-ph/0208184.
184. P. J. Armitage, Astrophys. J. **665**, 1381 (2007); arXiv:0705.3039.
185. R. I. Hynes and E. L. Robinson, Astrophys. J. **749**, 3 (2012); arXiv:1201.5680.
186. R. D. Alexander, C. J. Clarke, and J. E. Pringle, Mon. Not. R. Astron. Soc. **369**, 229 (2006); astro-ph/0603254.
187. J. Hernández, N. Calvet, C. Briceño, L. Hartmann, A. K. Vivas, J. Muzerolle, J. Downes, L. Allen, and R. Gutermuth, Astrophys. J. **671**, 1784 (2007); arXiv:0709.0912.
188. C. Salyk, G. A. Blake, A. C. A. Boogert, and J. M. Brown, Astrophys. J. **699**, 330 (2009).
189. K. France, E. Schindhelm, E. B. Burgh, G. J. Herczeg, G. M. Harper, A. Brown, J. C. Green, J. L. Linsky, H. Yang, H. Abgrall, D. R. Ardila, E. Bergin, T. Bethell, J. M. Brown, N. Calvet, et al., Astrophys. J. **734**, 31 (2011); arXiv:1104.0670.
190. K. France, J. L. Linsky, F. Tian, C. S. Froning, and A. Roberge, Astrophys. J. Lett. **750**, L32 (2012); arXiv:1204.1976.
191. E. A. Bergin, Y. Aikawa, G. A. Blake, and E. F. van Dishoeck, in *Protostars and Planets V,* Ed. by Bo Reipurth and D. Jewitt, Space Science Series (Univ. of Arizona Press, 2007), p. 751; astro-ph/0603358.
192. T. R. Ayres, J. L. Linsky, T. Simon, S. Jordan, and A. Brown, Astrophys. J. **274**, 784 (1983).
193. S. A. Matthews, D. R. Williams, K.-L. Klein, E. P. Kontar, D. M. Smith, A. Lagg, S. Krucker, G. J. Hurford, N. Vilmer, A. L. MacKinnon, V. V. Zharkova, L. Fletcher, I. G. Hannah, P. K. Browning, D. E. Innes, et al., Exp. Astron. **33**, 237 (2012).
194. K. G. Strassmeier, Astron. Astrophys. Rev. **17**, 251 (2009).
195. J.-F. Donati and S. Catala, Astron. Astrophys. **277**, 123 (1993).
196. K. G. Strassmeier, Astron. Astrophys. **281**, 395 (1994).
197. J. L. Linsky, R. Bushinsky, T. Ayres, and K. France, Astrophys. J. **754**, 69 (2012); arXiv:1205.6498.
198. J. L. Linsky, R. Bushinsky, T. Ayres, J. Fontenla, and K. France, Astrophys. J. **745**, 25 (2012); arXiv:1109.5653.
199. A. Reiners, M. Schüssler, and V. M. Passegger, Astrophys. J. **794**, 144 (2014); arXiv:1408.6175.
200. D. Shulyak, D. Sokoloff, L. Kitchatinov, and D. Moss, Mon. Not. R. Astron. Soc. **449**, 3471 (2015); arXiv:1503.04971.
201. E. M. Burbidge, G. R. Burbidge, W. A. Fowler, and F. Hoyle, Rev. Mod. Phys. **29**, 547 (1957).
202. S. Sneden, J. J. Cowan, and R. Gallino, Ann. Rev. Astron. Astrophys. **46**, 241 (2008).
203. C. Travaglio, R. Gallino, E. Arnone, J. Cowan, F. Jordan, and C. Sneden, Astrophys. J. **601**, 864 (2004); astro-ph/0310189.
204. K. Farouqi, K.-L. Kratz, L. I. Mashonkina, B. Pfeiffer, J. J. Cowan, F.-K. Thielemann, and J. W. Truran, Astrophys. J. Lett. **694**, L49 (2009); arXiv:0901.2541.
205. K. Farouqi, K.-L. Kratz, B. Pfeiffer, T. Rauscher, F.-K. Thielemann, and J. W. Truran, Astrophys. J. **712**, 1359 (2010); arXiv:1002.2346.
206. A. Arcones and F. Montes, Astrophys. J. **731**, 5 (2011); arXiv:1007.1275.
207. S. Wanajo, H.-T. Janka, and B. Muller, Astrophys. J. Lett. **726**, L15 (2011), 1009.1000.
208. T. Ryabchikova, L. Mashonkina, and M. Sachkov, in *Ultraviolet Universe II,* Ed. by B. M. Shustov, M. E. Sachkov, and E. Yu. Kil'pio (Yanus, Moscow, 2008), p. 168 [in Russian].
209. I. U. Roederer, J. E. Lawler, J. J. Cowan, T. S. Beers, A. Frebel, I. I. Ivans, H. Schatz, J. S. Sobeck, and S. Sneden, Astrophys. J. Lett. **747**, L8 (2012); arXiv:1202.2378.
210. I. U. Roederer, Astrophys. J. **756**, 36 (2012); arXiv:1207.0518.
211. I. U. Roederer, H. Scliatz, J. E. Lawler, T. S. Beers, J. J. Cowan, A. Frebel, I. I. Ivans, S. Sneden, and J. S. Sobeck, Astrophys. J. **791**, 32 (2014); arXiv:1406.4554.
212. I. U. Roederer, J. E. Lawler, J. S. Sobeck, T. S. Beers, J. J. Cowan, A. Frebel, I. I. Ivans, H. Schatz, S. Sneden, and I. B. Thompson, Astrophys. J. Suppl. Ser. **203**, 27 (2012); arXiv:1210.6387.
213. G. Michaud, Astrophys. J. **160**, 641 (1970).
214. T. Ryabchikova and F. Leblanc, Astrophys. Space Sci. **335**, 77 (2011).
215. L. Mashonkina, T. Ryabchikova, A. Ryabtsev, and R. Kildiyarova, Astron. Astrophys. **495**, 297 (2009); arXiv:0811.3614.
216. F. LeBlanc, D. Monin, A. Hui-Bon-Hoa, and P. H. Hauschildt, Astron. Astrophys. **495**, 937 (2009).
217. T. Ryabchikova, F. LeBlanc, and D. Shulyak, in *Magnetic Stars* (Spec. Astrophys. Observ., Nizhnii Arkhyz, Russia, 2011), p. 69.
218. I. Iben, J. B. Kaler, J. W. Truran, and A. Renzini, Astrophys. J. **264**, 605 (1983).
219. T. Rauch, K. Werner, P. Quinet, and J. W. Kruk, Astron. Astrophys. **577**, A6 (2015).
220. K. Werner, T. Rauch, E. Ringat, and J. W. Kruk, Astrophys. J. **753**, L7 (2012).
221. U. Heber, Ann. Rev. Astron. Astrophys. **47**, 211 (2009).
222. S. J. O'Toole and U. Heber, Astron. Astrophys. **452**, 579 (2006), astro-ph/0603069.
223. P. Chayer, M. Fontaine, G. Fontaine, F. Wesemael, and J. Dupuis, Baltic Astron. **15**, 131 (2006).
224. N. Naslim, C. S. Jeffery, N. T. Behara, and A. Hibbert, Mon. Not. R. Astron. Soc. **412**, 363 (2011); arXiv:1010.5146.

225. N. Naslim, C. S. Jeffery, A. Hibbert, and N. T. Behara, Mon. Not. R. Astron. Soc. **434**, 1920 (2013); arXiv:1407.7668.
226. M. D. Reed, S. D. Kawaler, R. H. Østensen, S. Bloemen, A. Baran, J. H. Telting, R. Silvotti, S. Charpinet, A. C. Quint, and G. Handler, Mon. Not. R. Astron. Soc. **409**, 1496 (2010); arXiv:1008.0582.
227. T. M. Brown, T. Lanz, A. V. Sweigart, M. Cracraft, I. Hubeny, and W. B. Landsman, Astrophys. J. **748**, 85 (2012); arXiv:1201.4070.
228. S. Yi, Y.-W. Lee, J.-H. Woo, J.-H. Park, P. Demarque, and A. Oemler, Jr., Astrophys. J. **513**, 128 (1999); astro-ph/9810022.
229. Z. Han, P. Podsiadlowski, and A. E. Lynas-Gray, Mon. Not. R. Astron. Soc. **380**, 1098 (2007); arXiv:0704.0863.
230. D. W. Atlee, R. J. Assef, and C. S. Kochanek, Astrophys. J. **694**, 1539 (2009); arXiv:0808.0010.
231. V. P. Utrobin and N. N. Chugai, Astron. Astrophys. **491**, 507 (2008); arXiv:0809.3766.
232. S. J. Smartt, Ann. Rev. Astron. Astrophys. **47**, 63 (2009); arXiv:0908.0700.
233. R. M. Quimby, S. R. Kulkarni, M. M. Kasliwal, A. Gal-Yam, I. Arcavi, M. Sullivan, P. Nugent, R. Thomas, D. A. Howell, and E. Nakar, Nature **474**, 487 (2011); arXiv:0910.0059.
234. M. Nicholl, S. J. Smartt, A. Jerkstrand, S. A. Sim, C. Inserra, J. P. Anderson, C. Baltay, S. Benetti, K. Chambers, and T.-W. Chen, arXiv:1505.01078 (2015).
235. J. J. Hester, Ann. Rev. Astron. Astrophys. **46**, 127 (2008).
236. V. P. Utrobin and N. N. Chugai, Astron. Astrophys. **575**, A100 (2015); arXiv:1411.6480.
237. P. Lundqvist, C. Fransson, and R. A. Chevalier, Astron. Astrophys. **162**, L6 (1986).
238. J. Sollerman, P. Lundqvist, D. Lindler, R. A. Chevalier, C. Fransson, T. R. Gull, C. S. J. Pun, and G. Sonneborn, Astrophys. J. **537**, 861 (2000); astro-ph/0002374.
239. M. Y. Marov, V. I. Shematovich, and D. V. Bisicalo, Space Sci. Rev. **76**, 1 (1996).
240. R. E. Johnson, M. R. Combi, J. L. Fox, W.-H. Ip, F. Leblanc, M. A. McGrath, V. I. Shematovich, D. F. Strobel, and J. H. Waite, Space Sci. Rev. **139**, 355 (2008).
241. V. I. Shematovich, Solar Syst. Res. **42**, 473 (2008).
242. D. V. Bisikalo, V. I. Shematovich, J.-C. Gérard, E. Jehin, A. Decock, D. Hutsemékers, J. Manfroid, and B. Hubert, Astrophys. J. **798**, 21 (2015).
243. L. Roth, J. Saur, K. D. Retherford, D. F. Strobel, P. D. Feldman, M. A. McGrath, and F. Nimmo, Science **343**, 171 (2014).
244. A. Stiepen, A. I. F. Stewart, S. K. Jain, N. M. Schneider, J. Deighan, J. S. Evans, M. H. Chaffin, W. E. McClintock, J. T. Clarke, and G. R. Holsclaw, in *46th Lunar and Planetary Science Conference,* Lunar and Planetary Inst. Technical Report, Vol. 46 (2015), p. 2937.
245. M. Meurant, J. S. Gérard, B. Hubert, V. Coumans, V. I. Shematovich, D. V. Bisikalo, D. S. Evans, G. R. Gladstone, and S. B. Mende, J. Geophys. Res. (Space Phys.) **108**, 1247 (2003).
246. J.-C. Gérard, B. Bonfond, D. Grodent, A. Radioti, J. T. Clarke, G. R. Gladstone, J. H. Waite, D. Bisikalo, and V. I. Shematovich, J. Geophys. Res. (Space Phys.) **119**, 9072 (2014).
247. J.-C. Gérard, B. Hubert, D. V. Bisikalo, and V. I. Shematovich, J. Geophys. Res. **105**, 15795 (2000).
248. J.-C. Gérard, V. I. Shematovich, D. V. Bisikalo, and D. Lummerzheim, Ann. Geophys. **23**, 1473 (2005).
249. V. I. Shematovich, D. V. Bisikalo, J.-C. Gérard, C. Cox, S. W. Bougher, and F. Leblanc, J. Geophys. Res. (Planets) **113**, E02011 (2008).
250. V. I. Shematovich, D. V. Bisikalo, C. Diéval, S. Barabash, G. Stenberg, H. Nilsson, Y. Futaana, M. Holmstrom, and J.-C. Gérard, J. Geophys. Res. (Space Phys.) **116**, A11320 (2011).
251. V. I. Shematovich, Astrophys. Space Sci. **335**, 3 (2011).
252. V. I. Shematovich, D. V. Bisikalo, G. Stenberg, S. Barabash, C. Diéval, and J.-C. Gérard, J. Geophys. Res. (Space Phys.) **118**, 1231 (2013).
253. H. U. Frey, S. B. Mende, T. J. Immel, J.-C. Gérard, B. Hubert, S. Habraken, J. Spann, G. R. Gladstone, D. V. Bisikalo, and V. I. Shematovich, Space Sci. Rev. **109**, 255 (2003).
254. A. Vidal-Madjar, A. Lecavelier des Etangs, J.-M. Désert, G. E. Ballester, R. Ferlet, G. Hébrard, and M. Mayor, Nature **422**, 143 (2003).
255. A. Vidal-Madjar, A. Lecavelier des Etangs, J.-M. Désert, G. E. Ballester, R. Ferlet, G. Hébrard, and M. Mayor, Astrophys. J. Lett. **676**, L57 (2008); arXiv:0802.0587.
256. L. Ben-Jaffel, Astrophys. J. Lett. **671**, L61 (2007); arXiv:0711.1432.
257. A. Vidal-Madjar, J.-M. Désert, A. Lecavelier des Etangs, G. Hébrard, G. E. Ballester, D. Ehrenreich, R. Ferlet, J. C. McConnell, M. Mayor, and C. D. Parkinson, Astrophys. J. Lett. **604**, L69 (2004); astro-ph/0401457.
258. L. Ben-Jaffel and S. Sona Hosseini, Astrophys. J. **709**, 1284 (2010); arXiv:0912.1409.
259. J. L. Linsky, H. Yang, K. France, C. S. Froning, J. C. Green, J. T. Stocke, and S. N. Osterman, Astrophys. J. **717**, 1291 (2010); arXiv:1005.1633.
260. R. V. Yelle, Icarus **170**, 167 (2004).
261. V. I. Shematovich, D. V. Bisikalo, and D. E. Ionov, in *Characterizing Stellar and Exoplanetary Environments,* Ed. by H. Lammer and M. Khodachenko, Vol. 411 of *Astrophysics and Space Science Library* (Springer International, Switzerland, 2015), p. 105.
262. H. Lammer, K. G. Kislyakova, M. Holmstrom, M. L. Khodachenko, and J.-M. Grießmeier, Astrophys. Space Sci. **335**, 9 (2011).

263. L. Fossati, C. A. Haswell, C. S. Froning, L. Hebb, S. Holmes, U. Kolb, C. Helling, A. Carter, P. Wheatley, and A. Collier Cameron, Astrophys. J. Lett. **714**, L222 (2010); arXiv:1005.3656.
264. A. García Muñoz, Planet Space Sci. **55**, 1426 (2007).
265. T. T. Koskinen, R. V. Yelle, M. J. Harris, and P. Lavvas, Icarus **226**, 1695 (2013); arXiv:1210.1543.
266. H. I. M. Lichtenegger, H. Lammer, J.-M. Grießmeier, Y. N. Kulikov, P. von Paris, W. Hausleitner, S. Krauss, and H. Rauer, Icarus **210**, 1 (2010).
267. A. Lecavelier des Etangs, A. Vidal-Madjar, J. C. McConnell, and G. Hébrard, Astron. Astrophys. **418**, LI (2004); astro-ph/0403369.
268. S. A. Haswell, L. Fossati, T. Ayres, K. France, C. S. Froning, S. Holmes, U. S. Kolb, R. Busuttil, R. A. Street, and L. Hebb, Astrophys. J. **760**, 79 (2012); arXiv:1301.1860.
269. A. Vidal-Madjar, S. M. Huitson, V. Bourrier, J.-M. Désert, G. Ballester, A. Lecavelier des Etangs, D. K. Sing, D. Ehrenreich, R. Ferlet, and G. Hébrard, Astron. Astrophys. **560**, A54 (2013); arXiv:1310.8104.
270. D. Bisikalo, P. Kaygorodov, D. Ionov, V. Shematovich, H. Lammer, and L. Fossati, Astrophys. J. **764**, 19 (2013); arXiv:1212.2779.
271. M. Leitzinger, P. Odert, Y. N. Kulikov, H. Lammer, G. Wuchterl, T. Penz, M. G. Guarcello, G. Micela, M. L. Khodachenko, and J. Weingrill, Planet Space Sci. **59**, 1472 (2011).
272. M. Holmström, A. Ekenbäck, F. Selsis, T. Penz, H. Lammer, and P. Wurz, Nature **451**, 970 (2008); arXiv:0802.2764.
273. V. Bourrier and A. Lecavelier des Etangs, Astron. Astrophys. **557**, A124 (2013); arXiv:1308.0561.
274. K. France, S. S. Froning, J. L. Linsky, A. Roberge, J. T. Stocke, F. Tian, R. Bushinsky, J.-M. Désert, P. Mauas, and M. Vieytes, Astrophys. J. **763**, 149 (2013); arXiv:1212.4833.
275. L. Fossati, D. Bisikalo, H. Lammer, B. Shustov, and M. Sachkov, Astrophys. Space Sci. **354**, 9 (2014).

Translated by D. Gabuzda